NASA CONTRACTOR REPORT

NASA CR-1521

OPTICAL ALTIMETER RECEIVER SYSTEMS STUDY AND DESIGN FOR A SPACEBORNE LASER ALTIMETER

by Howard C. Salwen, Herbert G. Coles, and David R. Torrealba

Prepared by
ADCOM, A Teledyne Company
Cambridge, Mass.
for Electronics Research Center

NATIONAL AERONAUTICS AND SPACE ADMINISTRATION • WASHINGTON, D. C. • FEBRUARY 1970

OPTICAL ALTIMETER RECEIVER SYSTEMS STUDY AND DESIGN FOR A SPACEBORNE LASER ALTIMETER

By Howard C. Salwen, Herbert G. Coles,
and David R. Torrealba

Prepared under Contract No. NAS 12-2058 by
ADCOM
A Teledyne Company
Cambridge, Mass.

for Electronic Research Center

NATIONAL AERONAUTICS AND SPACE ADMINISTRATION

For sale by the Clearinghouse for Federal Scientific and Technical Information
Springfield, Virginia 22151 – Price $3.00

CONTENTS

ILLUSTRATIONS

SECTION 1

INTRODUCTION

This document constitutes the Final Report prepared for NASA Electronic Research Center, Cambridge, Massachusetts, under Contract Number NAS12-2058 entitled Optical Altimeter Receiver Systems Study and Design for a Spaceborne Laser Altimeter.

Objective of the Program

The objective of this study program is to provide a complete design and specification for an optical altimeter receiver. In particular, the system under consideration consists of a satellite borne laser transmitter and receiver oriented such that the transmitted beam is normal to the earth's surface. The laser is a mode locked Neodymium-YAG device with pulse repetition rate of 5 kHz to 200 MHz. The receiver photo-multiplier is a device which provides detected laser pulse width of 1 to 10 nsec. It is anticipated that the width of the laser beam at sea level will be on the order of 10m. and the laser beam speed over the water surface will be on the order of 6.9 km/sec. The distance measurement accuracy desired of the system is 10 cm.

The tasks to be performed to accomplish the goals of this study effort are specified as follows:

1. Perform a complete design and performance parameter analysis and trade off study of the subsystems employing the above introductory information.

2. Determine and specify the minimum required signal/noise ratio at the output of the photomultiplier detector for accurate distance measurements over the ocean surface from a satellite.

3. Design and specify optimal state-of-the-art leading edge and split gas laser altimeter receiver signal processing and handling subsystems to operate within the range of the parameters specified in the introduction. Specify the commercial sources for all components of the design.

4. Perform such laboratory experiments as are needed to confirm the validity and accuracy of analytical design predictions.

Summary of the Report

The report responds directly to the task statements above. Section 2 considers the effect of received signal statistics on distance measurement errors. The tracking gate width and pulse width are optimized with respect to receiver signal photon rate background rate and the statistical fluctuation in the distance measured due to surface irregularity and/or propagation anomalies.

The results of Sec. 2 shows that the tracking error as a function of input photon rate (i. e., Signal-to-Noise Ratio) can be arbitrarily reduced by providing sufficiently long averaging time. Section 3 derives the limitation on averaging time or, equivalently, noise bandwidth imposed by the dynamics of range as a function of time for the tracking configurations under consideration. Specifically the design and performance obtainable with second and third order digital filter implementation are analyzed and presented.

Section 4 presents design definition of system parameters for the laser mean-sea level altimeter. The system parameter and design characteristics which are considered include:

1) tracking loop compensation implementations

2) loop noise bandwidth

3) rate-aiding requirements

4) loop acquisition characteristic, and

5) special loop stability considerations.

A second system configuration is also considered. This is a lunar ranging tracker which transmits and receives in the vicinity of Boston, Massachusetts, and which utilizes an array of corner cube retroreflectors located on the surface of the moon.

Section 5 discussed the circuit design factors associated with the development of split-gate and leading-edge trackers for use with the mean-sea level altimeter. A laboratory effort is described which was conducted to determine the limitations of standard printed circuit techniques and commercial components in building split-gates and leading-edge gates.

Section 6 describes a simulation program which was prepared during the study effort to demonstrate the validity of the theoretical performance analyses and to provide a convenient means of experimentation with the system parameters.

Section 7 presents conclusions and recommendations.

SECTION 2

NOISE ANALYSIS

This section presents an analysis of the performance of optical range tracking loops in the presence of fluctuations due to statistical variations in the number of photons returned from the target to be tracked and in the number of background photons. Two gating models are assumed. One model represents the situation in which the probability of observing a photon due to signal or background is small so that the probability of two photons overlapping in a particular sampling interval is almost nil. Another model is analyzed which represents the case of a large number of photons returned per sampling interval. It is shown that the results obtained are applicable in both cases without modification.

Gates for Non-Overlapping Photons

It is reasonable to assume that the number of photons returned during any given sampling interval is less than or equal to one in several directly practical situations. This will be the case, for example, in the Mean-Sea Level (MSL) Laser Altimeter. In general, the assumption of non-overlapping photon returns is reasonable when the system is severely power limited and/or when a high PRF is used.

The MSL Laser Altimeter optical design parameters are chosen to produce roughly $n_s = 15$ signal photon returns per sec. while transmitting at a PRF of roughly 5-10 kHz. The background photon rate is on the order of $n_b = 10^{+4}$ per sec. to 10^{+5} per sec. as a function of the time of day. Thus, assuming 10 nsec. gates at a rate, $r = 10,000$ per sec. the total number of background photons per sec. is on the order of, $rn_b\tau_g = 1\text{-}10$, where τ_g is the gate width.

Since it is assumed that the photons do not overlap at the photodetector, the "width" of the returned photons as seen at the output of the photodetector is determined by the characteristics of the photodetector. For the purposes of analysis, it is assumed that the transmitted pulse duration is on the order of 0.1 nsec. and the duration of the response of the photodetector to the arrival of a single photon is 1-3 nsec.

In the case of the MSL Laser Altimeter, the "width" of the returned pulse, averaged over a large number of returns, is determined by the character of the reflecting surface, i.e., the sea-state. Each photon return originates from a particular spot on the water's surface

and the vertical displacement of this spot from MSL is a mean zero random variable. Thus, the round trip time delay of each photon return is a random variable with a mean determined by the satellite altitude relative to the MSL and variance determined by the sea-state. For the purposes of illustration it is assumed that the distribution of time delays is rectangular. The width of the rectangular distribution is assumed to be on the order of 10 nsec. This corresponds to a maximum wave peak-to-trough separation of 5 ft. Other distributions will be considered later in the discussion.

It is clear that a leading-edge tracking gate is not appropriate for the MSL Altimeter with the parameters assumed above because such a device would tend to track the crests of the waves rather than the MSL. Furthermore, implementation of a leading-edge tracker would be complicated by the random delay fluctuations of the returned pulses because these fluctuations are much larger than appropriate gate widths of optical leading-edge trackers. On the other hand, a leading-edge tracker could be useful in those applications where the photodetector output pulses are much wider than the random delay fluctuations due to sea-state or any other cause. Typically, the gate width of a leading-edge tracker is an order of magnitude smaller than the pulse duration. Thus, the pulse duration must be several order of magnitude larger than the delay fluctuations for this technique to be used effectively.

Split-Gate Tracker

A split-gate tracker suitable for the MSL altimeter is shown in block diagram form in Fig. 1. Briefly, the device operates as follows: The voltage controlled oscillator (VCO) generates a trigger pulse train which is synchronized with the laser returns. When the trigger pulse train lags or leads the laser returns an appropriate voltage is generated at the output of the integrator which after filtering is used to correct the phase of the trigger pulse train.

Details of the split-gate implementation can be altered to take advantage of the quantized nature of the returns. For example, Fig. 2 shows a split-gate design which produces a digital phase error output. In this device the loop error signal is generated by counting and taking the difference of the number of received photons which arrive in each half of the gate during the digital loop sampling interval, τ_s. The difference is found by sensing the state of the integrator (sample-and-hold) at the end

of each gate interval and making a tertiary decision. Specifically, it can be decided that no photon was received during the gate interval. This will be the case most of the time. Or, if a photon did arrive, it is decided that the photon arrived before or after the center of the gate. Then, the threshold circuit either increments or decrements the digital up-down counter accordingly. The contents of the counter are read out and the counter is reset at the sampling rate, $1/\tau_s$. This rate is related to the loop tracking bandwidth which, in turn, is determined by constraints imposed by noise and target dynamics. The contents of the counter are filtered in a digital filter and used to advance or retard the phase of the VCO output so that the split gate is aligned with the center of gravity of the returned photons, on the average.

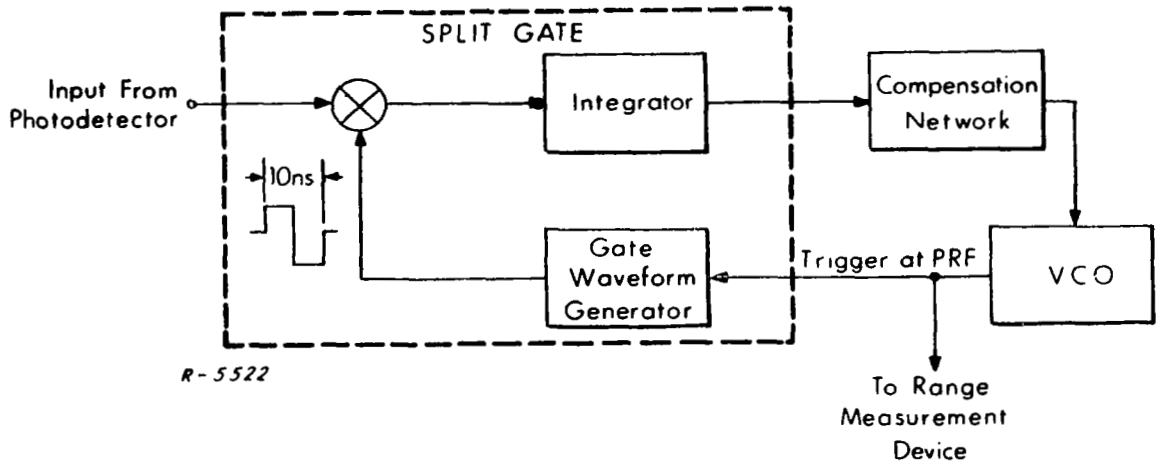

Fig. 1 Split-Gate Tracking Loop

Simplified Analysis

The analysis of this type of gate is somewhat simplified if the effect of background photons are excluded from the calculations. This effect will be added later in section entitled "Effect of Background Radiation," p.

The average number of signal photons observed in the gate in one sampling interval is defined to be $n_s\tau_s$ and is Poisson distributed. Thus, the probability that k photons are observed in τ_s second is

$$p(k,\tau_s) = \frac{(n_s\tau_s)^k e^{-n_s\tau_s}}{k!} \qquad (1)$$

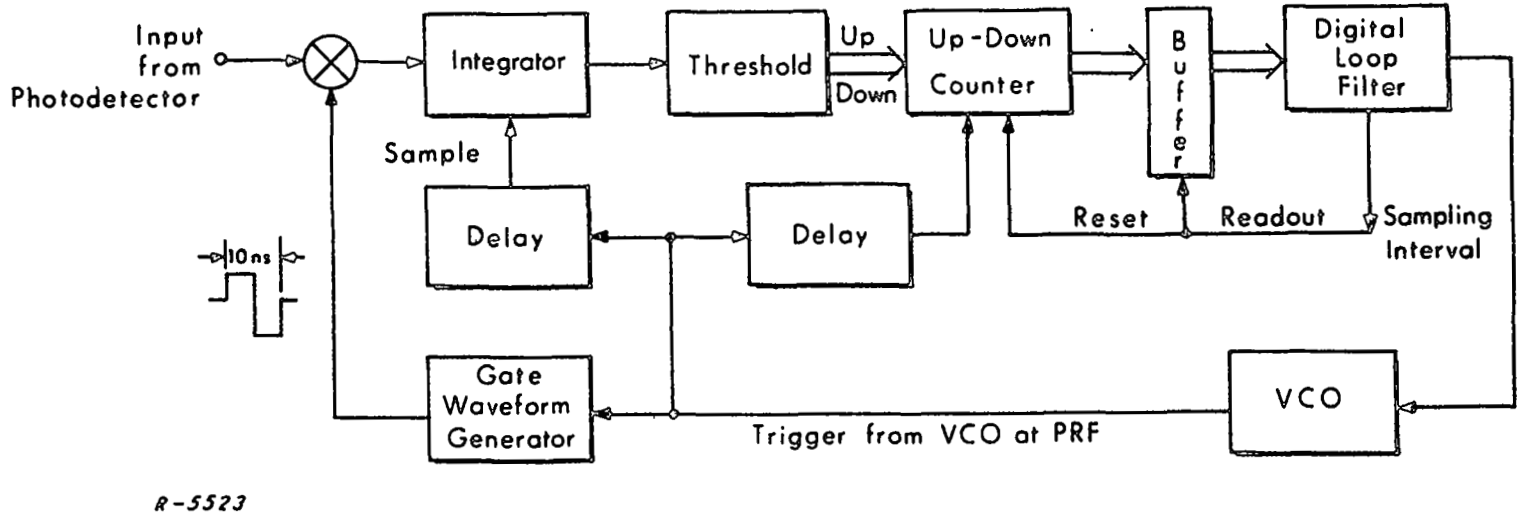

Fig. 2 Modified Split-Gate Design

provided that the gate is properly aligned. The number of photons in the early and late halves of the gate, k_+ and k_-, are also poisson distributed with mean $n_s\tau_s/2$. The counter forms the difference k_+ and k_- which clearly has zero mean when the gate is properly aligned. This situation is shown in Fig. 3. The joint probability density of k_+ and k_- is simply the product of their probabilities because these events are independent. Thus,

$$p(k_+, k_-) = p(k_+)p(k_-) = \frac{\left(\frac{n_s\tau_s}{2}\right)^{k_+} e^{-\frac{n_s\tau_s}{2}}}{k_+!} \quad \frac{\left(\frac{n_s\tau_s}{2}\right)^{k_-} e^{-\frac{n_s\tau_s}{2}}}{k_-!} \tag{2}$$

and the expected value of the difference is

$$\begin{aligned} E(k_+ - k_-) &= \sum_{k_+=0}^{\infty} \sum_{k_-=0}^{\infty} (k_+ - k_-)\, p(k_+, k_-) \\ &= \sum_{k_+=0}^{\infty} k_+ p(k_+) - \sum_{k_-=0}^{\infty} k_- p(k_-) \\ &= \frac{n_s\tau_s}{2} - \frac{n_s\tau_s}{2} = 0 \end{aligned} \tag{3}$$

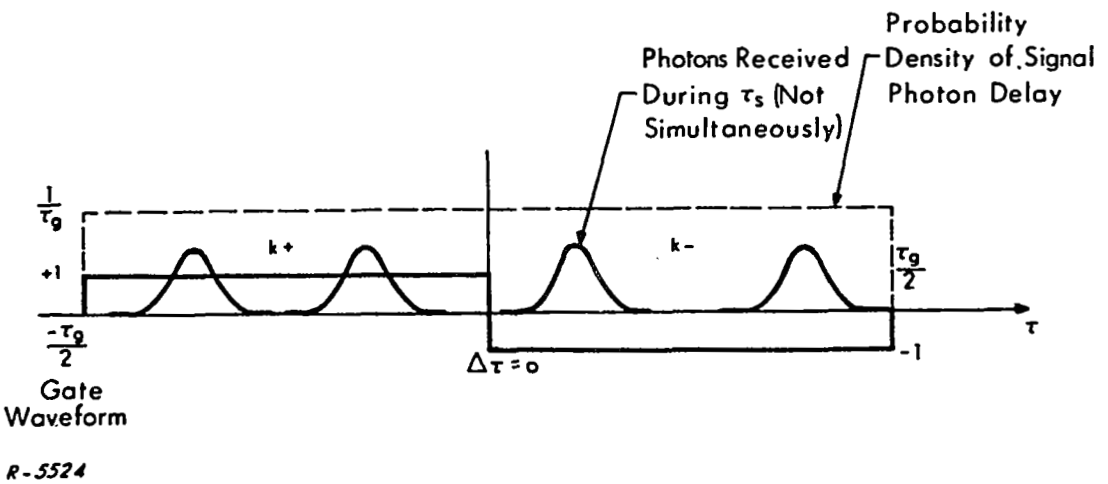

Fig. 3 Photons Counted During τ_s

With mean equal to zero, the variance of the difference is computed to be

$$E[(k_+ - k_-)^2] = \sum_{k_+=0}^{\infty} \sum_{k_-=0}^{\infty} (k_+^2 - 2k_+k_- + k_-^2)\, p(k_+)p(k_-)$$

$$= \left[\left(\frac{n_s\tau_s}{2}\right) + \left(\frac{n_s\tau_s}{2}\right)^2\right] - 2\left(\frac{n_s\tau_s}{2}\right)^2 + \left[\left(\frac{n_s\tau_s}{2}\right) + \left(\frac{n_s\tau_s}{2}\right)^2\right]$$

$$= n_s\tau_s \qquad (4)$$

Therefore, the contents of the counter has rms fluctuation, $\sigma_n = \sqrt{n_s\tau_s}$. These random counter fluctuations will cause random fluctuations of the gate position, $\Delta\tau_{rms}$, which constitute ranging measurement noise. Thus, the effect of counter fluctuations, σ_n, on the gate position must be determined. It is simpler, conceptually, to derive this relationship by determining the gate sensitivity, i.e., the steady-state error signal (counter contents) which would be produced given that the gate is displaced by a small amount, $\Delta\tau$. Then, substituting the random counter fluctuations due to the statistical nature of the signal for the steady-state error component in the sensitivity relationship, the resulting delay fluctuations, $\Delta\tau_{rms}$, can be determined.

The sensitivity of the gate to a displacement $\Delta\tau$ is found as follows: Assume the gate is moved $\Delta\tau$ to the left in Fig. 3. The mean value of k_+ is still

$$E(k_+/\Delta\tau) = \frac{n_s\tau_s}{2} = n_s\tau_s \frac{1}{\tau_g} \frac{\tau_g}{2} \qquad (5)$$

The mean value of k_- is reduced because part of the late gate is outside the region in which photon returns are expected, i.e.,

$$E(k_-/\Delta\tau) = n_s\tau_s \frac{1}{\tau_g}\left(\frac{\tau_g}{2} - \Delta\tau\right) \qquad (6)$$

Thus, the expected value of the contents of the counter, $k_+ - k_-$, given a displacement $\Delta\tau$, is

$$E[(k_+ - k_-)/\Delta\tau] = n_s\tau_s \frac{\Delta\tau}{\tau_g} \tag{7}$$

Combining Eqs. (4) and (7), it is found that the rms fluctuations of the content of the counter, σ_n, will be interpreted as delay fluctuations with rms value given by

$$\Delta\tau_{rms} = \frac{\tau_g\sigma_n}{n_s\tau_s} = \frac{\tau_g}{\sqrt{n_s\tau_s}} \tag{8}$$

In a two-way ranging system this corresponds to a range error of

$$\Delta r_{rms} = \frac{c\Delta\tau_{rms}}{2} = \frac{c\tau_g}{2\sqrt{n_s\tau_s}} \tag{9}$$

There are several assumptions implicit in this result, namely:

1) effects of background and dark current are ignored

2) signal photon delay fluctuations are rectangularly distributed with width τ_w

3) the gate width τ_g is chosen equal to τ_w

4) photon returns do not overlap and are counted separately.

Effect of Background Radiation

The effect of background radiation is easily added to the result, Eq. (9), using the same calculation technique. Assume a background photon rate n_b and pulse rate r. The average number in each gate is $n_b\tau_g$ and the average total number per sample interval is $rn_b\tau_g\tau_s$. Again, the number of background photons is poisson distributed and mean in the early and late halves of the gate is $rn_b\tau_g\tau_s/2$ regardless of gate displacement. Denoting the number of background photons in the early and late

halves of the gate is $rn_b\tau_g\tau_s/2$ regardless of gate displacement. Denoting the number of background photons in the early and late halves of the gate by ℓ_+ and ℓ_- respectively, the variance of the contents of the counter is

$$\begin{aligned} E[(k_+ + \ell_+ - k_- - \ell_-)^2] &= E(k_+^2) + 2E(k_+\ell_+) \\ &-2E(k_+k_-) - 2E(k_+\ell_-) + E(\ell_+^2) - 2E(\ell_+k_-) \\ &-2E(\ell_+\ell_-) + E(k_-^2) + 2E(k_-\ell_-) + E(\ell_-^2) \end{aligned} \tag{10}$$

Again, it has been assumed that k_+, k_-, ℓ_+, and ℓ_- are statistically independent variables, and following the same procedure as in Eq. (4), it is found that

$$E[(k_+ + \ell_+ - k_- - \ell_-)^2] = (n_s + rn_b\tau_g)\tau_s \tag{11}$$

Thus, the rms count fluctuations including the effect of background, are

$$\sigma_n = \sqrt{(n_s + rn_b\tau_g)\tau_s} \tag{12}$$

and substituting in Eqs. (8) and (9) yields

$$\Delta r_{rms} = \frac{c\tau_g\sqrt{(n_s + rn_b\tau_g)\tau_s}}{2n_s\tau_s}, \quad \tau_g = \tau_w \tag{13}$$

When independent range measurements are desired every τ_i seconds where $\tau_i = m\tau_s$, $m = 1, 2, \ldots$, the results of m measurements can be averaged in τ_i seconds yielding an error

$$\Delta r(\tau_i) = \frac{\Delta r_{rms}}{\sqrt{m}} = \frac{c\tau_g\sqrt{(n_s + rn_b\tau_g)}}{2\sqrt{m\tau_s}\, n_s} = \frac{c\tau_w\sqrt{(n_s + rn_b\tau_w)\tau_i}}{2n_s\tau_i}, \quad \tau_g = \tau_w \tag{14}$$

Typically the loop integration time, or equivalently, the independent sample rate, is expressed in terms of the loop noise bandwidth, B_n. In particular, the integration time, τ_i, is approximately inversely proportional to the loop noise bandwidth.

Before further generalizing of the range error expression, Eq. (14), it is of interest to examine the behavior of the error as a function of the number of signal and background photons per decision, i.e., $N_s = n_s\tau_i$ and $N_b = rn_b\tau_g\tau_i$. Figure 4 shows a plot of the function $\sqrt{N_s+N_b/N_s}$ vs. N_b with N_s as a parameter. It is interesting to note, from Fig. 4, that the tracker shows relatively little degradation as the number of background photons are increased. For example, consider the cases in which $N_s = 10$ and $N_b = 0$ or $N_b = 90$. Over this range of background photons, the accuracy factor varies only by a factor of 3.16.

Further Generalization

The analysis leading to Eq. (14) assumes that gate duration τ_g and the width of the delay distribution due to sea-state, τ_w, are equal. For practical reasons, such as acquisition considerations, it is often desirable to make the gate width wider than the expected width of the pulse return. This is case analyzed next.

The number of signal photons and background photons has the same statistics as described above. So Eq. (12) for the rms fluctuation of the counter output remains valid in this case. However, the gate sensitivity calculation, Eqs. (5-7) must be altered. In particular, as shown in Fig. 5, the count k_+ will not be independent of displacement Δ_τ. Thus, Eq. (5) is replaced by

$$E(k_+/\Delta\tau) = \frac{n_s}{\tau_w}\,\tau_s\left(\frac{\tau_w}{2} + \Delta\tau\right) \tag{15}$$

and Eq. (6) is replaced by

$$E(k_-/\Delta\tau) = \frac{n_s}{\tau_w}\,\tau_s\left(\frac{\tau_w}{2} - \Delta\tau\right) \tag{16}$$

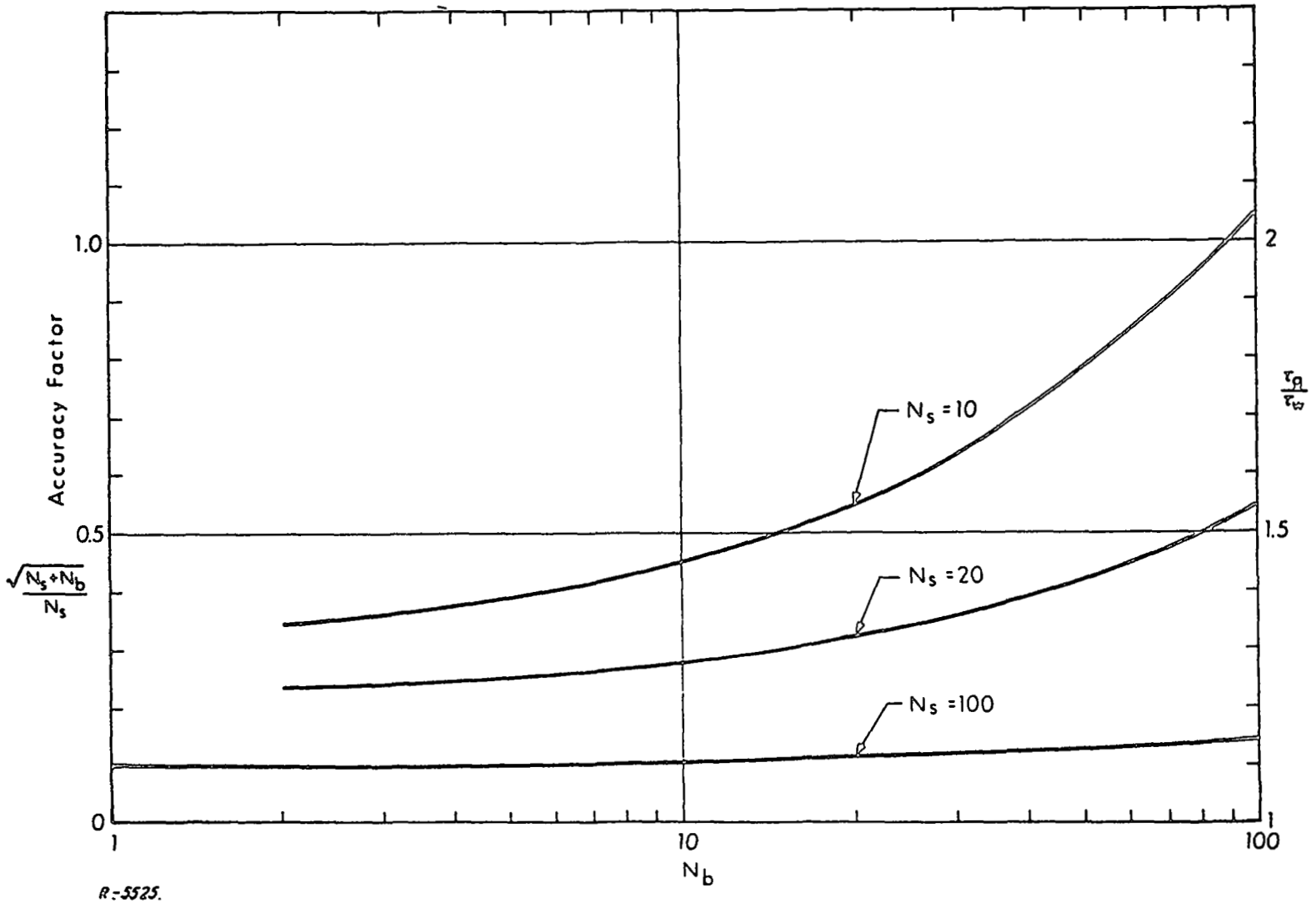

Fig. 4 Laser Tracker Accuracy Factor $\frac{\sqrt{N_b + N_s}}{N_s}$ vs N_b and Gate Width Criterion $\frac{\tau_g}{\tau_w} = \frac{\sqrt{N_b + N_s}}{N_s} + 1$

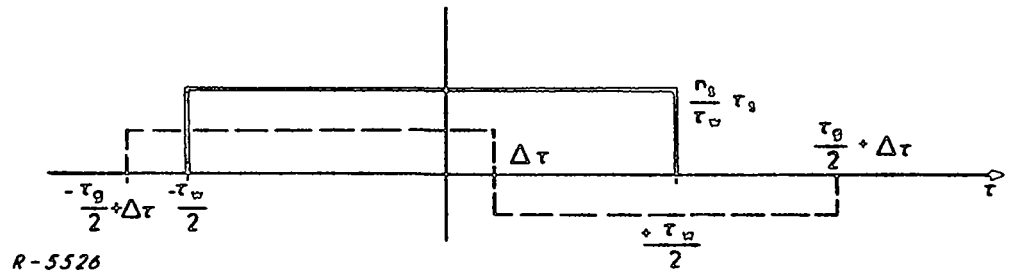

Fig. 5 Modified Gate

Therefore

$$E(k_+ - k_-/\Delta\tau) = \frac{2n_s\tau_s\Delta\tau}{\tau_w} \tag{17}$$

Following the same procedure as before, the rms ranging error is found to be

$$\Delta r_{rms} = \frac{c\tau_w\sqrt{(n_s+rn_b\tau_g)\tau_s}}{2(2n_s\tau_s)} \tag{18}$$

or

$$\Delta r(\tau_i) = \frac{c\tau_w\sqrt{(n_s+rn_b\tau_g)\tau_i}}{4n_s\tau_i} \tag{19}$$

At first glance the accuracy predicted by Eq. (19) appears to be better by a factor of 2 than that predicted by Eq. (14). But it should be remembered that $\tau_g > \tau_w$ in Eq. (19). An exact comparison can be made under conditions of small error. Namely, the ratio of Eq. (14) over Eq. (19) constitutes an improvement given by

$$I = \frac{c\tau_w\sqrt{(n_s+rn_b\tau_w)\tau_i}}{2n_s\tau_i} \times \frac{4n_s\tau_i}{c\tau_w\sqrt{(n_s+rn_b\tau_g)\tau_i}} \tag{20}$$

$$= 2\sqrt{\frac{(n_s+rn_b\tau_w)}{(n_s+rn_b\tau_g)}} \qquad \tau_g > \tau_w$$

Equation (20) shows that in the absence of background photons, the wider gate tracker does provide double the accuracy. It is important to note than when τ_g is just slightly larger than τ_w Eq. (20) does not apply. It only applies when $\Delta\tau < (\tau_g - \tau_w)/2$, i.e., all the signal photon expected arrival times fall with the gate. It is thus concluded that τ_g should be made as small as possible while still maintaining this criterion. Since the gate timing error, $\Delta\tau$, is a random variable, this criterion can only be established on an average basis. For example, τ_g can be chosen such that the criterion is maintained as long as the gate displacement is within its 1_σ value. That is,

$$\frac{(\tau_g - \tau_w)}{2} = \Delta\tau = \frac{\tau_w\sqrt{(n_s + rn_b\tau_g)\tau_i}}{2n_s\tau_i} \tag{21}$$

Equation (21) need not be solved exactly for τ_g because the magnitude of the expression on the right is typically known in terms of the system specification. The tracking accuracy goal for the M. S. L. altimeter is approximately 1 ft., which corresponds to $\Delta\tau$ = 2 nsec. Alternatively, Eq. (21) can be recast in terms of the accuracy factor $\sqrt{N_s + N_b}/N_s$, i.e.,

$$\frac{\tau_g - \tau_w}{2} = \frac{\tau_w}{2}\left[\frac{\sqrt{N_s + N_b}}{N_s}\right] \tag{22}$$

or

$$\frac{\tau_g}{\tau_w} = 1 + \frac{\sqrt{N_s + N_b}}{N_s} \tag{23}$$

A plot of the ratio τ_g/τ_w which meets the 1_σ criterion is simply added to Fig. 4. Since gate widths on the order of $2\tau_w$ are sufficiently wide to satisfy the 1_σ criterion mentioned above under all conditions shown in Fig. 4, it is clear from Eq. (20) that improvement factors greater than $\sqrt{2}$ are achievable when $N_b > N_s$ and that improvement factors approaching 2 are achievable in some cases.

High Intensity Returns

Not all laser range tracking systems are photon limited as was the case above. When the average power is high enough and the P. R. F. is low enough, the output of the receiver's photodetector will consist of the sum of many overlapping photon responses. The threshold device and up/down counter of Fig. 2 are inappropriate in this application because the output of the integrator is not quantized. Thus, the threshold device and up/down counter, which served as an elementary A/D converter in the photon limited case, must be replaced by a conventional A/D converter if a digital filter compensation network is used. Typically, however, an analog active filter would be implemented, in which case the output of the integrator could be used directly as shown in Fig. 1. A split-gate tracker realized in this way would be almost equivalent to an ordinary radar except that the signal and background are described by poisson statistics. The results derived above still hold although individual signal and background photons are not actually counted as was assumed. Instead, the integrator output provides an analog error signal which is, again, proportional to the difference of the number of photons received in the early and late halves of the gate. Of course, this output is available after every received pulse. Therefore, the sampling interval, τ_s, has little meaning or importance. For this case, τ_s can be as short as $1/r$.

It is reasonable to assume that the number of signal photons, N_s, received per pulse is quite large. Therefore, the noisy nature of the signal photons will produce negligibly small errors. In the absence of background photons and when the pulse width is narrow (say, 20 nsec or less), the ranging accuracy would be determined by equipment limitations or possibly by propagation anomalies. On the other hand, it is reasonable to assume that the background radiation is intense because such a situation would justify the expense of providing the high signal photon intensity.

When the received pulse is rectangular of duration τ_p, the ranging accuracy is given by a slightly modified form of Eq. (19), namely

$$\Delta r(\tau_i) = \frac{c\tau_p\sqrt{(n_s+rn_b\tau_g)\tau_i}}{4n_s\tau_i} \qquad (24)$$

The assumption associated with Eq. (19) are again valid for the above expression. Equation (24) may be simplified for the case of high background photon intensities. That is

$$\Delta r(\tau_i) = \frac{c\tau_p}{4}\sqrt{\frac{1}{n_s\tau_i}+\frac{rn_b\tau_g}{n_s^2\tau_i}} \approx \frac{c\tau_p}{4\sqrt{\frac{n_s^2\tau_i}{rn_b\tau_g}}} \tag{25}$$

Effect of Pulse Shape on Accuracy

Up to this point, the received pulse shape has been assumed to be rectangular. Of course, other possibilities exist and two will be considered in this section. These are shown in Fig. 6. The pulse shapes can also be considered as probability distributions in the non-overlapping case.

Figure 6a shows a raised cosine shape which is an approximation to the Gaussian pulse shape. Such waveforms are appropriate for the analysis of returns from extended homogeneous scatterers. The Gaussian shape may also be used to represent the laser transmitter output.

The second pulse shape, shown in Fig. 6b, corresponds to the return from an extended scatterer with two main points of reflection. It is believed that such scattering will occur off the water. Thus, it may be appropriate for analysis of the MSL altimeter.

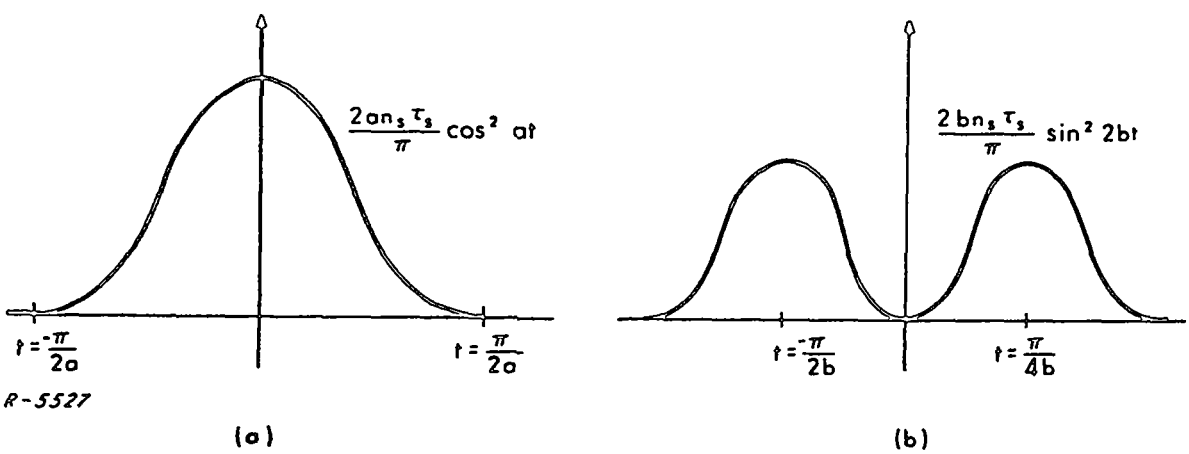

Fig. 6 Possible Pulse Return Shapes

The calculation to determine the accuracy of the tracker assuming these alternate pulse shapes is carried out in the same manner as that of the rectangular pulse. The main difference, in terms of results, is in the sensitivity calculation. Assuming a gate width $\tau_g < \pi/a$, a displacement $\Delta\tau$ produces a net output of the integrator given by

$$e_{int}(\Delta\tau) = -\frac{2an_s\tau_s}{\pi}\left[-\int_{-(\tau_g/2)+\Delta\tau}^{0}\cos^2 a t\,dt - \int_{0}^{\Delta\tau}\cos^2 a t\,dt + \int_{\Delta\tau}^{(\tau_g/2)+\Delta\tau}\cos^2 a t\,dt\right]$$

$$= \frac{2an_s\tau_s}{\pi}\left[\frac{\left(-\frac{\tau_g}{2}+\Delta\tau\right)}{2} + \frac{\sin 2a\left(-\frac{\tau_g}{2}+\Delta\tau\right)}{4a}\right. \tag{26}$$

$$\left. - 2\left(\frac{\Delta\tau}{2}\right) - \frac{2\sin 2a\Delta\tau}{4a} + \frac{\left(\frac{\tau_g}{2}+\Delta\tau\right)}{2} + \frac{\sin 2a\left(\frac{\tau_g}{2}+\Delta\tau\right)}{4a}\right]$$

$$= \frac{n_s\tau_s}{\pi}\left[\sin 2a\Delta\tau(\cos a\tau_g - 1)\right]$$

for small $\Delta\tau$ this is approximated by

$$e_{int}(\Delta\tau) \sim \frac{n_s\tau_s}{\pi} 2a\Delta\tau(\cos a\tau_g - 1) \tag{27}$$

This is, as before, set equal to the rms integrator fluctuations due to the random nature of the signal and background, which is given by a modified form of Eq. (11). The modification is required because the signal photon mean rate n_s is a function of the gate width in the system presently under consideration. As the gate is narrowed the number of signal photons counted in the interval τ_s is given by

$$n_s(\tau_g)\tau_s = \int_{-\tau_g/2}^{\tau_g/2} 2a\,\frac{n_s\tau_s}{\pi}\cos^2 a t\,dt \tag{28}$$

$$= \frac{n_s\tau_s}{\pi}\left[a\tau_g + \sin a\tau_g\right]$$

which approaches $n_s\tau_s$ as τ_g approaches π/a. The rms ranging accuracy is thus,

$$\Delta r_{rms} = \frac{c\pi\sqrt{\frac{n_s\tau_s}{\pi}[a\tau_g + \sin a\tau_g] + rn_b\tau_g\tau_s}}{4a(1 - \cos a\tau_g)n_s\tau_s} \tag{29}$$

The optimum gate width is a function of the signal-to-background ratio N_b/N_s. When the background is small $\tau_g = \pi/a$ is best. As this ratio is increased, the optimum gate width is reduced. Digital calculations of Eq. (29) with various values of the ratio N_b/N_s have been performed and it is found that when $N_b/N_s \leq 1$, $\tau_g = \pi/a$ is optimum and when $1 < N_b/N_s \leq 3000$ $\tau_g = 0.9\,\pi/a$ is roughly optimum. (Calculations with $N_b/N_s > 3000$ were not undertaken.)

Analysis of the second pulse shape in Fig. 6b is performed in the same manner. Assuming a gate width $\tau_g < \pi/b$, a displacement $\Delta\tau$ produces a net output of the integrator given by

$$e_{int}(\Delta\tau) = \frac{2bn_s\tau_s}{\pi}\left[-\int_{-(\tau_g/2)+\Delta\tau}^{0} \sin^2 2bt\,dt - \int_{0}^{\Delta\tau} \sin^2 2bt\,dt + \int_{\Delta\tau}^{(\tau_g/2)+\Delta\tau} \sin^2 2bt\,dt\right]$$

$$= -\frac{2n_s\tau_s}{4\pi}[\sin 4b\Delta\tau(1 - \cos 2b\tau_g)] \tag{30}$$

For small $\Delta\tau$ this is approximated by

$$e_{int}(\Delta\tau) \approx \frac{n_s\tau_s 2b\Delta\tau}{\pi}(1 - \cos 2b\tau_g) \tag{31}$$

Modification of Eq. (11) is again necessary and, similar to Eq. (28), the mean number signal photons is given by

$$n_s(\tau_g)\tau_s = \int_{-\tau_g/2}^{\tau_g/2} \frac{2bn_s\tau_s}{\pi} \sin^2 2bt$$

$$= \frac{n_s\tau_s}{2\pi} [2b\tau_g - \sin 2b\tau_g] \tag{32}$$

The rms ranging accuracy for this pulse shape is thus

$$\Delta r_{rms} = \frac{c\pi\sqrt{\frac{n_s\tau_s}{2\pi} [2b\tau_g - \sin 2b\tau_g] + rn_b\tau_g\tau_s}}{2b(1 - \cos 2b\tau_g)n_s\tau_s} \tag{33}$$

The optimum gate is again a function of the signal-to-background ratio N_b/N_s. The optimum gate for small background levels is, of course, $\tau_g = \pi/b$. But, as the background increases to a significant level, $N_b/N_s > 10$, the optimum gate width is reduced to roughly $0.45\pi/b$. Note that the shape of the pulse in Fig. 6b is substantially different from that typically encountered in tracking problems. Therefore, it is probably true that further improvements can be obtained by optimizing the split gate shape to this received pulse shape. Substantial improvement will not be obtained in this way for the Gaussian pulse shape of Fig. 6a because the early-late gate configuration is, in fact, nearly optimum for that shape.

SECTION 3

DYNAMICS ANALYSIS

Section 2 has discussed the error in a laser ranging system introduced by background noise and by the statistical characteristics of the signal. Clearly these errors can be reduced by increasing the integration time of the range tracking loop. This section discusses the constraints imposed on loop integration time by range dynamics, whereas background noise and signal fluctuations establish a lower bound on integration time, the dynamic characteristics of range impose an upper bound on the integration time. The design of range tracking loops typically incorporates a trade-off exercise in which the loop integration time is selected to minimize the combined effects of noise and dynamics.

The discussion below considers two compensation techniques which are suitable for application in the range tracking loops of Sec. 2. Specifically, the design of and performances obtainable with 2nd and 3rd order digital filters are analyzed and presented. Extensive discussion of typical 2nd order analog filters is notable by its absence. However, data concerning this frequently employed compensation technique is available from numerous sources[1,2] and therefore will not be discussed, in detail, here.

Design of Digital Compensation Networks for Analog Tracking Loop

A typical analog 2nd order compensation network for a tracking filter is a lead-lag network with transfer function given by

$$F(s) = \frac{\tau_1 s + 1}{\tau_2 s + 1} \tag{34}$$

A more desirable form of lead-lag compensation can be realized digitally, that is,

$$F(s) = \frac{\tau_1 s + 1}{s} \tag{35}$$

1. Gardner, F.M., Phaselock Techniques, John Wiley & Sons, 1966.
2. Salwen, H. and Warren, D. "Design Criteria for Radar Tracking Systems," Final Report. Prepared under Contract ER-13-784 for NASA/ERC April 19, 1968.

Thus the digital filter can perform a perfect integration (characterized by the "s" in the denominator) while the analog filter provides a good, but imperfect, approximation to integration. This slight difference has little effect on the closed loop response or the closed loop noise bandwidth. However, it does have an important effect on the dynamic error response of the loop, as will be shown below.

The digital implementation of the 2nd order compensation is shown in Fig. 7. Figure 7a shows the operations to be performed in block diagram form and Fig. 7b shows the actual digital implementation.

The compensation network for a 3rd order tracking loop requires a transfer function of the form

$$F(s) = \frac{(\tau_1 s + 1)^2}{s^2} \tag{36}$$

Thus, the implementation consists basically of a cascade of two units of the type shown in Fig. 7.

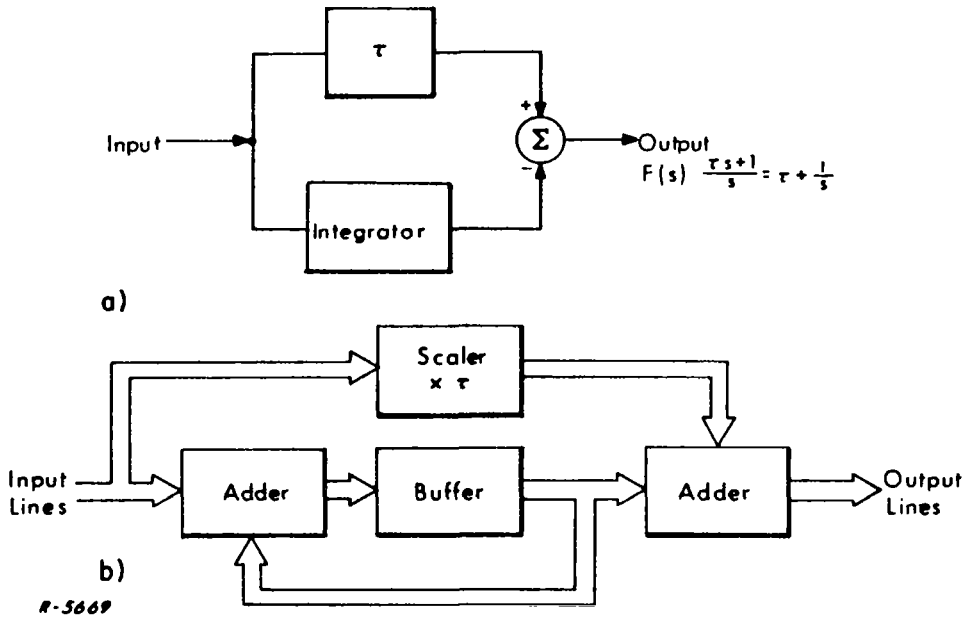

Fig. 7 Digital Filter Implementation

Some additional circuitry is required in the case of the 2nd order filter to provide initialization and/or piloting of the loop. The 3rd order filter also requires such circuitry and in addition requires some circuit modifications during loop acquisition to provide stable operation during acquisition. These details will be discussed further below.

2nd Order Loop Performance

The open loop response of a second order tracking loop is given by

$$G(s) = \frac{K}{s} F(s) = \frac{K(\tau s + 1)}{s^2} \tag{37}$$

where K is the total open loop gain which in turn is the product of the VCO gain, K_V, the gain of the compensation network, K_A, and the gain of the split gate, K_ϕ. The VCO is assumed to be a perfect integrator of phase (time delay) and has a transfer function, K_V/s. The closed loop response of the 2nd order tracker is

$$H(s) = \frac{G(s)}{1 + G(s)} = \frac{K(\tau s + 1)}{s^2 + K\tau s + K} \tag{38}$$

The noise bandwidth (double sided) is given by

$$B_n = \frac{1}{2\pi j} \int_{-\infty}^{\infty} |H(s)|^2 \, ds \tag{39}$$

Substituting Eq. (37) into Eq. (38) yields

$$B_n = \frac{K\tau^2 + 1}{2\tau} \tag{40}$$

Assuming a specific damping factor for the loop, such as critical damping, provides a means for relating K and τ. Thus, assuming that the denominator in Eq. (38) has the form $s^2 + 2\xi\omega_n s + \omega^2$,

$$2\xi\omega_n = K\tau$$

and (41)

$$\omega_n^2 = K$$

With $\xi = 0.707$, it is found that

$$\frac{K\tau}{2\sqrt{K}} = 0.707$$

or

$$K\tau^2 = 2 \tag{42}$$

Finally it is concluded that a 2nd order critically camped loop employing the type of compensation described by Eq. (35) has

$$B_n = \frac{3}{2\tau} = \sqrt{\frac{9K}{8}} \tag{43}$$

The open loop response characteristic is shown in Fig. 8.

The dynamic capabilities of tracking loops are typically expressed in terms of steady-state errors due to position, velocity and acceleration inputs. The steady-state error is found with the aid of the final value theorem, i.e.,

$$\lim_{s\to 0} sF(s) = \lim_{t\to\infty} f(t) \tag{44}$$

where F(s) and f(t) are a Fourier transform pair. Given an excitation X(s) the steady-state error is

$$\lim_{s\to 0} sX(s)E(s) = \lim_{t\to\infty} e(t) \tag{45}$$

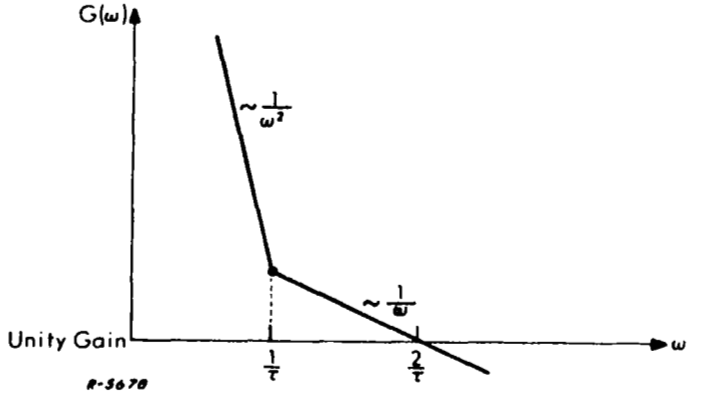

Fig. 8 Open Loop Response of a 2nd Order Loop

where E(s) is the error response of the loop defined by

$$E(s) = 1 - H(s) = \frac{1}{1 + G(s)} \tag{46}$$

The loop under consideration here has no steady-state error component to position inputs of the form $X(s) = X/s$ or velocity inputs of the form $X(s) = V/s^2$. A steady-state error is produced by an acceleration input $X(s) = A/s^3$, and the error is given by

$$\lim_{s \to 0} s \frac{A}{s^3} \frac{s^2}{s^2 + K\tau s + K} = \frac{A}{K} = \frac{1.125A}{B_n^2} \tag{47}$$

It is interesting to note that an analog 2nd order loop using the type of compensation of Eq. (34) has a steady-state error due to velocity given by V/K. In addition, the acceleration error of such loops consists of a term similar to that of Eq. (47) and a growing term of the form At/K. Thus, the digital filter provides improved dynamic performance compared to a similar analog 2nd order filter with the same loop noise bandwidth.

3rd Order Loop Performance

A 3rd order loop filter provides further improvement for a given loop noise bandwidth at the expense of added system complexity. The complexity of such systems is associated with their unstable characteristics under conditions of reduced gain. Such conditions do, in fact, arise during acquisition of the tracking loop. The accepted method of achieving stable operation of 3rd order locked loops is to simply modify the compensation network to 2nd order for the duration of the acquisition process. When acquisition is accomplished the network is changed to the 3rd order configuration. This operation is difficult to achieve with analog compensation networks because a transient which results from the change in configuration can unlock the loop. The digital filter approach offers the possibility of transient-free alteration of the compensation characteristics.

The open loop response of a suitable third-order tracking loop is given by

$$G(s) = \frac{K}{s} F(s) = \frac{K(\tau s + 1)^2}{s^3} \tag{48}$$

The closed loop response is given by

$$H(s) = \frac{G(s)}{1 + G(s)} = \frac{K(\tau s + 1)^2}{s^3 + K\tau^2 s^2 + 2K\tau s + K} \tag{49}$$

The double-sided noise bandwidth is again given by Eq. (39) and is found to be

$$B_n = \frac{2K^2\tau^5 + 3K\tau^2}{4K\tau^3 - 2} \tag{50}$$

The damping factor, ξ, and the relationship between K, τ and the damping factor, ξ, are not as easily derived compared to the 2nd order analysis. The denominator may be factored to form

$$s^3 + K\tau^2 s^2 + 2K\tau s + K = (s + b)(s^2 + 2as + 2a^2) \tag{51}$$

This is accomplished after much algebraic manipulation and it is found that for critical damping of the quadratic factor of Eq. (51), $K \approx 4.121/\tau^3$ with $b = 1/1.414\tau$ and $a = 1.707/\tau$.

The resulting open loop transfer function is shown in Fig. 9. Examination of Fig. 9 shows the mechanism of instability in this 3rd order loop. Namely, when the effective open loop gain of the system is reduced (as is the case during acquisition), the unity gain point of the system moves up into the region where the open loop gain slope is roughly proportional to

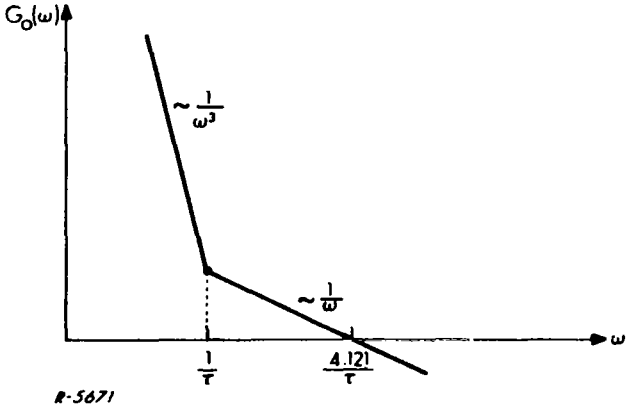

Fig. 9 3rd Order Open Loop Transfer Function

$1/\omega^3$ and the phase is approaching -270 degrees. Somewhere along the way, unity gain with -180° phase shift can be established and this will result in oscillation of the system.

Substituting the critical damping constraint, $K \approx 4/\tau^3$ into Eq. (50) yields a simplified expression for the noise bandwidth, i.e.,

$$B_n \approx \frac{3.2}{\tau} \tag{52}$$

The dynamic performance obtainable with the 3rd order system is derived in the same manner as that presented in Eqs. (45) through (47) for the 2nd order system. In the 3rd order system,

$$E(s) = 1 - H(s) = \frac{s^3}{s^3 + K\tau^2 s^2 + 2K\tau s + K} \tag{53}$$

The steady-state errors due to position, velocity, and acceleration inputs are readily found to be zero. The first non-trivial steady-state dynamic error is produced by a rate of change of acceleration, J. Specifically the error due to a jerk, J, is

$$\lim_{s \to 0} s \frac{J}{s^4} \frac{s^3}{s^3 + K\tau^2 s^2 + 2K\tau s + K} = \frac{J}{K} \approx \frac{8.41J}{B_n^3} \tag{54}$$

Comparison of 2nd and 3rd Order Systems

The comparison of performances obtainable with the two compensation schemes outlined above may be carried out by assuming that both systems provide the same noise performance, i.e., both have the same noise bandwidth, B_n. Under these conditions, the 2nd order system has a time constant given by

$$\tau_c = \frac{3}{2B_n} \tag{55}$$

assuming that the system is critically damped. Assuming that the 3rd order system is factored as shown in Eq. (51), the resulting system will have a time constant controlled by the value of b. This time constant is

$$\tau_c \approx \frac{4.5}{B_n} \tag{56}$$

It is noted that the 3rd order system, as configured, has a longer settling time. This can be reduced somewhat by slightly reducing the loop gain, K, and readjusting τ to produce the desired noise bandwidth. When this is done, the conjugate poles of the denominator of the system function will no longer be critically damped. This is desirable in 3rd order systems because the time constant associated with the conjugate poles of Eq. (51) is roughly $\tau/1.707$ which is substantially shorter than that associated with the real axis pole, i.e., 1.414τ. Slight underdamping of the conjugate poles will result in a reduction of the overall settling time without jeopardizing system stability.

The dynamic performance obtainable with the 3rd order loop is clearly superior because it has no steady-state error with acceleration inputs while the 2nd order system has an error given by Eq. (47), namely $1.125A/B_n^2$. Furthermore, the steady-state error for a rate of change of acceleration is $8.4J/B_n^3$ for the 3rd order system, while the 2nd order jerk error grows without bound. This latter point does not imply that the second order system will produce infinite errors for jerk inputs because the rate of change of acceleration can only exist until the maximum acceleration is reached. At that time, the jerk must vanish or change sign.

The additional performance obtained with the 3rd order implementation is clearly at the expense of added system complexity. The decision as to which compensation to employ in a given situation is determined by analyzing the specific characteristics of a tracking mission. This analysis will be carried out in the next section.

SECTION 4

DESIGN DEFINITION

This section analyzes the characteristics of two tracking missions and provides range tracking system designs suitable for each. The first system is the MSL altimeter considered above which operates on board a satellite. The second system is a lunar ranging tracker which transmits and receives in the vicinity of Boston, Massachusetts, and which utilizes an array of corner cube retroreflectors located on the surface of the moon.

The system parameters and design characteristics which are considered include:

1) tracking loop compensation implementations

2) loop noise bandwidth

3) rate-aiding requirements

4) loop acquisition characteristics

and

5) special loop stability requirements.

Tracker Dynamic Requirements

Tracker dynamics requirements, in the case of the mean sea level (MSL) altimeter come from three sources, the variation in altitude of the satellite, the roughness of the ocean surface and the variations in the MSL itself. It is assumed that the MSL fluctuations are very slow and of very low amplitude. The effects of ocean roughness are considered as short term fluctuations about the slowly varying MSL. These need not be tracked by the loop. Instead, as discussed in Sec. 2, the loop split gate is made large enough to encompass this fluctuation in altitude and the loop averages it out. The variations in satellite altitude must be tracked and since these are also slowly varying, the altimeter will measure the sum of the MSL variations and the satellite altitude variations. In order to get an idea of the order of magnitude of these effects, a slightly elliptical orbit is assumed for the satellite instead of a circular orbit. Assuming an

eccentricity of $\pm R$ and an orbital period T, the two-way range fluctuations due to orbital ellipticity are roughly described by

$$\Delta R = 2R \sin 2\pi \frac{2}{T} t \tag{57}$$

The maximum acceleration and jerk associated with the fluctuation assuming T is on the order of 90 minutes and R = 10 nautical miles are, roughly,

$$\Delta \ddot{R} = 2R \left(\frac{4\pi}{T}\right)^2 = 2 \times 6 \times 10^4 \left(\frac{4 \times 3.14}{5400}\right)^2 = 0.65 \frac{\text{ft}}{\text{sec}^2} \tag{58}$$

and

$$\Delta \dddot{R} = 2R \left(\frac{4\pi}{T}\right)^3 = 2 \times 6 \times 10^4 \left(\frac{4 \times 3.14}{5400}\right)^3 = 1.5 \times 10^{-3} \frac{\text{ft}}{\text{sec}^2} \tag{59}$$

With the aid of the steady-state dynamic error results derived in Sec. 3, it is seen that a second order loop will have an acceleration error approaching

$$\Delta r = \frac{9\Delta \ddot{R}}{8B_n^2} \approx \frac{.73}{B_n^2} \text{ feet} \tag{60}$$

and a third order system with the same dynamic input given by Eq. (57) will have a jerk error approaching

$$\Delta r = \frac{8.41 \Delta \dddot{R}}{B_n^3} \approx \frac{12.6}{B_n^3} \times 10^{-3} \text{ feet} \tag{61}$$

Examination of Eqs. (60) and (61) yields that given a constraint on maximum permissible lag error, a substantially smaller loop noise bandwidth can be achieved with the third order technique. Assume a maximum lag error of $\Delta r = 1$, the second order loop noise bandwidth must exceed 0.85 Hertz while the third order system requires 0.2326 Hertz. This implies that for equal dynamic performance, the third order system provides 1.91 times the noise performance, i.e., a reduction in error due to noise by a factor of 1.91.

Equations (60) and (61) also show that dynamic error in such systems is a strong function of the loop noise/bandwidth, B_n. For example, increasing loop noise bandwidth by a factor of 2 increases the noise error by $\sqrt{2}$ but quadruples the dynamic performance in the second order system and produces an eight-fold improvement in the third order system. Thus, final selection of the compensation technique depends on the noise filtering requirements. If a B_n of 1 Hertz is satisfactory with respect to the noise, then clearly a second order loop should be chosen because it does meet the dynamic requirements. The third order system would provide dynamic performance far in excess of that required. On the other hand, if a B_n of 0.25 Hz is necessary to meet the noise performance requirements, then the second order system would not meet the dynamic requirements unaided while the third order system would. The selection process then consists of a qualitative tradeoff of the complexity associated with rate-aiding the second order system vs. the complexity associated with acquiring the third order system. For the case of the satellite-borne MSL altimeter, rate-aiding is particularly difficult because it involves a careful measurement of the satellite orbit parameters and communication of these parameters or the actual rate-aiding signal to the satellite.

A similar analysis may be carried out for the lunar ranging laser system. In this case, the predominant source of dynamics is the relative motion of the surfaces of the earth and the moon. The configuration is shown in Fig. 10. At the point where the range between the earth and moon, R(t), is a minimum the rate of change of range is zero and the acceleration is a maximum. In particular, the maximum acceleration is approximately 8.15×10^{-2} ft/sec^2. The maximum rate of change of acceleration occurs when the moon appears at the horizon. This tracking configuration is of little interest. Roughly half the maximum jerk is observed at an elevation of, say, 60°. Under this condition, the jerk is approximately 3×10^{-6} ft/sec^3. The lower signal levels encountered in the lunar tracking mission will necessitate a very narrow loop noise bandwidth. Assuming this to be 0.1 Hz, the second order loop will have a peak

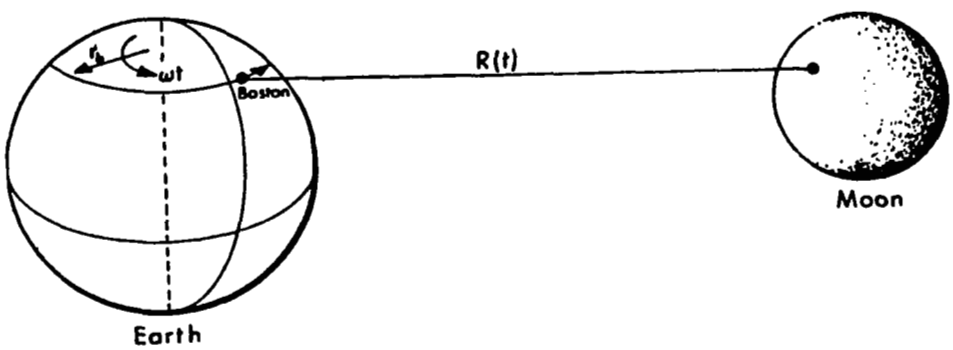

R-5681

Fig. 10 Earth-Moon Geometry

dynamic lag error which approaches 9.17 ft. A third order loop with the same loop noise bandwidth will have a peak lag error due to the rate of change of acceleration on the order of .025 ft.

The maximum permissible lag error for the lunar tracking mission is on the order of 1 ft. Thus, the second or loop performance is inadequate while the third order technique provides much more than the necessary performance.

Rate Aiding

The characteristics of the lunar tracking mission are such that rate-aiding of the tracking loops is particularly convenient. Advantage can be taken of the fact that the major component of range dynamics caused by the rotation of the earth is known, a priori. Assuming that the effect of the earth's rotation is removed to within 1% of its value, the acceleration lag error in the second order loop would be reduced to 0.09 ft. maximum. Rate-aiding is typically incorporated in the tracking loop as shown in Fig. 11.

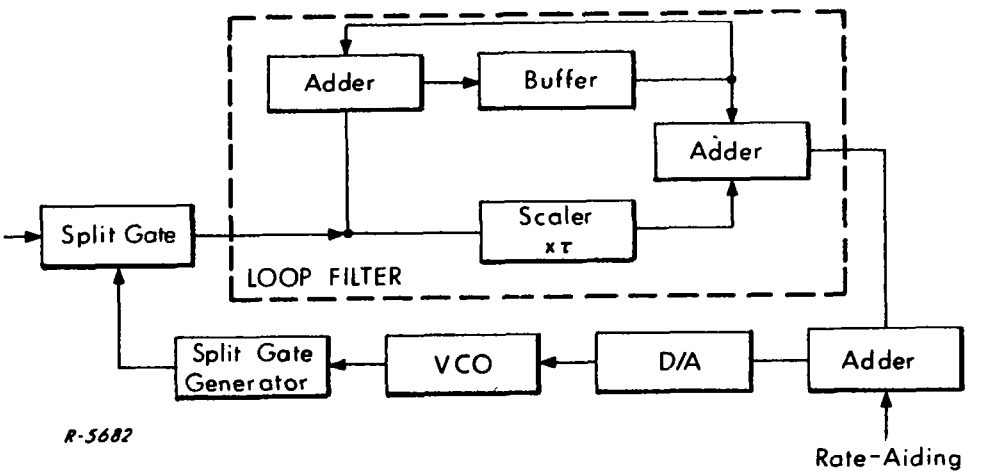

Fig. 11 Second-Order Loop with Rate-Aiding

The rate-aiding signal is simply added to the output of the loop filter. The rate-aiding signal is a sequence of pre-computed numbers which are proportional to the a priori estimate of the velocity component due to the earth's rotation.

The same rate-aiding effect is obtained by introducing an a priori estimate of the acceleration due to the earth's rotation as seen at the tracker. In this case, the acceleration aiding signal, which is again a sequence of pre-computed numbers, is added to the input of the accumulator as shown in Fig. 12.

Third Order Implementation

The calculations described above show that a third-order system does not require rate-aiding to provide the necessary performance. Nonetheless, because the third order system is modified to second order during the acquisition process, rate-aiding may again be required in this case.

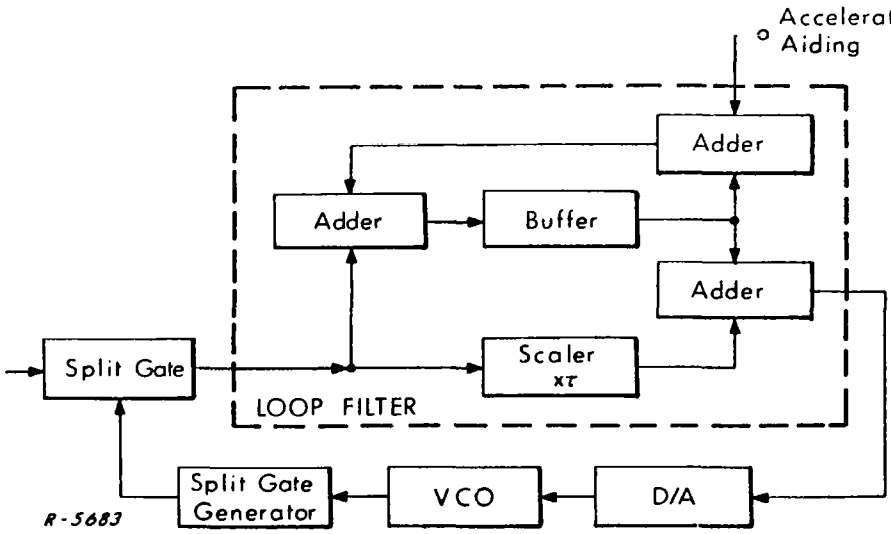

Fig. 12 Second-Order Loop with Acceleration Aiding

Rate -aiding during acquisition is avoided if the split-gate is widened and/or the loop noise bandwidth is widened for the duration of acquisition. Either of these modifications of system parameters results in increased noise error. However, this is allowable to a certain extent during acquisition.

Assuming that rate-aiding is not avoided during acquisition, the third order system will be configured as a second order loop exactly as shown in Figs. 11 or 12. After acquisition is completed and the split-gate pulse train more or less overlaps the received pulse train. the configuration is changed to the one shown in Fig. 13. The method for changing from one compensation to the other is also shown. Specifically, during acquisition the first compensation network is bypassed by disabling the buffer register output in the accumulator and at the same time changing the scaler multiplying factor from τ to unity. When acquisition is complete, the buffer output is enabled and the scaler factor changed to τ. Note that this operation does not simply constitute insertion of the additional components into the loop. In fact, the added network is appropriately initialized for approximately transient-free change-over because the accumulator of the added network is connected so that during acquisition *its contents always correspond to the most recent loop error.* Thus, when the buffer output is enabled, the buffer contains the most recent split-gate error number. It is noted that this number corresponds approximately to the most recent acceleration residual error of the second order configuration. Thus, the change-over will be virtually transient-free.

Advantages of Third Order Operation

The discussion above indicates that the third order implementation is more complex than the second order approach. It has been shown that in the third order operating mode the system will provide the necessary performance without rate-aiding. On the other hand, rate-aiding will probably be required during acquisition in the lunar mission.

The investment in complexity of the third order approach returns significant advantages in the lunar mission. The lunar mission is characterized by very low signal levels. In fact, it is possible that for appreciable time intervals no usable data will be received during the course of a tracking run. The third order loop, while it is tracking a usable signal, forms estimates of the initial delay, rate of change of delay and delay acceleration. These estimates are in effect stored in the two loop integrators and in the VCO. When input data is removed, the output of the loop, i. e., the phase of the VCO, continues to be the most recent quadratic estimate of the input. Under similar conditions, the second order configuration can only produce a linear estimate. Thus, in all probability the third order system will accumulate less error in a given time interval during which the data is unusable.

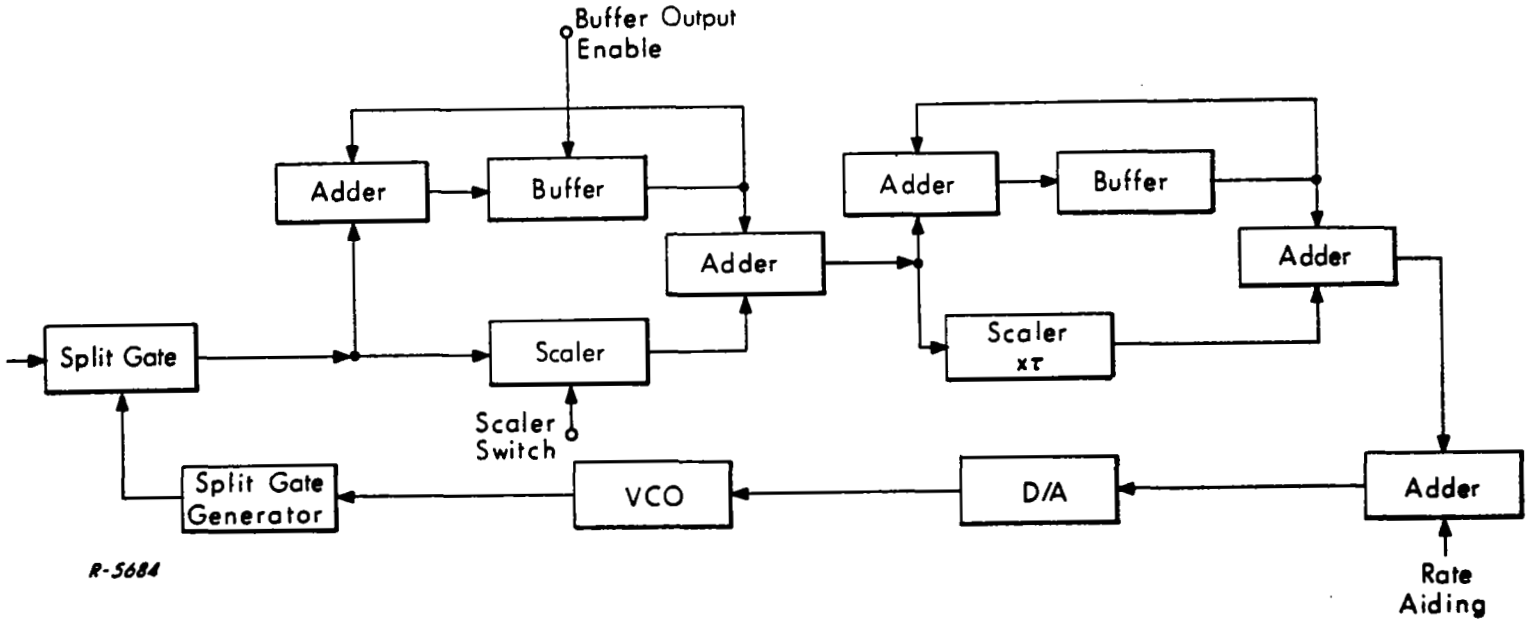

Fig. 13 Third-Order Configuration

Special Loop Stability Considerations

The question of loop stability during periods when the data is weak but usable must also be considered. In the discussion relevant to Fig. 9 of Sec. 3, it was noted that the loop will become unstable when the open loop gain is reduced. At the same time, the results of Sec. 2 show that the error gain of the split-gate detector is proportional to the number of photons observed during the measurement interval. Thus, it is clear that if the photon rate is reduced sufficiently relative to its mean rate, the loop will oscillate. The exact gain reduction required for oscillation to occur depends on the loop gain margin which in turn depends on the parameters of the loop, K and τ.

The probability of instability can be reduced by proportionally increasing the loop gain margin. Of course, this will result in slight degradation of the loop dynamic performance for a given noise performance.

Since the actual number of photons observed during each sampling interval is available in the tracking system, an additional safeguard against instability may be deployed. Specifically the error data may be normalized relative to the total number of counts received per sampling interval. This technique combined with substantial gain margin should result in stable operation with the photon rate varying over a 50-to-1 range.

In order to demonstrate the feasibility of this technique in particular, and the split-gate tracking technique in general, a digital simulation was performed. This effort and its results are described in Section 4.

Acquisition

Acquisition of the tracking loop is accomplished by sweeping the split-gate in time relative to the time of arrival of the incoming pulse returns. The sweep signal consists simply of a bias offset added to the rate aiding input signal of Fig. 11. This causes the VCO to operate at a slight higher or lower frequency relative to the rate-aid command, depending on the sign of the bias offset. The higher (or lower) frequency of the VCO results in motion of the split-gate in time relative to the received pulse train.

Given that there is some a priori knowledge of the round trip time to the target, the acquisition system can be implemented to sweep back and forth over the remaining range uncertainty interval until acquisition is achieved. When acquisition occurs, the error signal feedback around the tracking loop will cancel the effect of the acquisition bias offset at the rate-aid input point. Thus, in most cases, it is not necessary to remove the acquisition input. When this approach is taken, the acquisition process resumes immediately and automatically when the received signal drops out or is removed. On the other hand, some applications require that the system remain as close as possible to the last estimate of target range as a function of time. Then, the acquisition bias offset must be removed upon determination that acquisition has been achieved.

Acquisition Parameters

The time required to search a given range uncertainty region is determined by the gate width and the tracking loop bandwidth. Thus, it is concluded that the acquisition time is constrained by noise and dynamic performance requirements of the overall system.

Given an initial range uncertainty, R_i, the split-gate must be swept through a delay interval given by

$$\tau_{di} = \frac{2R_i}{c} \tag{62}$$

Now, the tracking loop response time is roughly on the order of $1/B_n$ seconds. The sweep must be slow enough so that the split-gate pulses overlap the received pulses for at least the loop response time. Thus, the sweep rate, sr, is determined to be the ratio of the split-gate width to the loop response time, i.e.,

$$sr \leq \tau_g B_n \text{ seconds per second.}$$

Finally, time required to search a range uncertainty interval R_i is

$$\tau_{ACQ} = \frac{\tau_{di}}{sr} = \frac{2R_i}{c\tau_g B_n} \tag{63}$$

For the case of the MSL altimeter, the initial range uncertainty may be as large as 500 ft., the split-gate width will be on the order of 10 nanoseconds, and the loop bandwidth will be on the order of 1 Hz. These parameters result in an acquisition time on the order of τ_{ACQ} = 100 seconds.

Acquisition Detection

An acquisition indicator is usually provided in ranging systems. Such a device is required in those systems where it is desirable to remove the acquisition bias offset after the acquisition process is completed.

When the ratio of signal photoelectrons to background photoelectrons is large, acquisition is easily detected by observation of the number of photomultiplier output pulses which occur in $1/B_n$ seconds. When the split-gate overlaps the incoming pulse train this number will exceed a predetermined threshold and acquisition is thus indicated. When the signal-to-background ratio is close to unity the number of events observed at the output of the photomultiplier will not increase significantly as the split-gates becomes aligned with the incoming pulse train.

Under conditions of low signal-to-background ratio, it is more desirable to observe the difference between the early and late arriving photons relative to the center of the split-gate. This difference is the contents of the up-down counter shown in Fig. 2. The effect of background photoelectrons is zero on the average with rms fluctuations given by $\sqrt{N_b}$ regardless of the split-gate position. On the other hand the average effect of signal produced photoelectrons is a function of the split-gate position. In particular, the average contents of the counter would be equal to the mean number of signal photons which arrive during the detection interval, N_s, provided that the split-gates overlap but are offset slightly relative to the incoming pulses. Consequently, as the split-gate center is swept passed the incoming pulses, the average contents of the up-down counter will first increase toward N_s, then decrease through zero toward $-N_s$, then increase back to zero again. Given that the sweep rate is slow enough, as specified above, the tracking loop will establish control of the gate position before the received pulses are completely passed by the split-gate.

SECTION 5

COMPUTER SIMULATION

PHOTON is a FORTRAN program for simulating a phase-locked loop whose input consists of detected photon arrivals. Figure 14 is a simplified flow diagram of the overall program. The initialization stage of the program accepts the operating parameters for this program from the computer teletype console and scales and/or converts the parameters to the correct units. These parameters include switches which enable or disable the target motion, the change from second to third order loop filter, and the acquisition sweep.

In addition to the initialization stage, the program, shown in Fig. 14, is composed of three nested loops: the main program loop (index M) the phase-locked loop (index L), and the phase detector (index I). One iteration through the main program loop corresponds to one "real time" second of operation of the photon phase-locked loop simulator. Computation in each of the three loops proceeds over a one second period during which the effective computation rate is 20 per second in the phase-locked loop and 5000 per second in the phase detector.

In one iteration of the main loop, the phase detector stage simulates photon arrivals, develops a phase-error signal, and counts the photons observed, and computes the difference between early and late photons (relative to the local oscillator phase). The photon count obtained is used in the next iteration of the main loop. The phase-locked loop (filter and VCO stages) operates on the photon count from the previous iteration of the main loop and develops the local oscillator phase signal for use by the phase detector.

Phase Detector

The phase detector stage, shown in Fig. 15, simulates the arrival of photons by comparing the output (modulo 10000) of a random number generating subroutine (RANDU) with a table of five digit random numbers (IRAN) whose length is given by the mean photon rate (MEAN). If a comparison occurs, counter J is incremented and the photon is counted.

Subroutine RANDU was specially written for the SEL 810B in its assembly language. This subroutine simulates a feedback shift register, 32 bits long. Therefore, $2^{32}-1$ random integers are generated before the sequence begins to repeat, providing that the feedback taps have been properly selected.

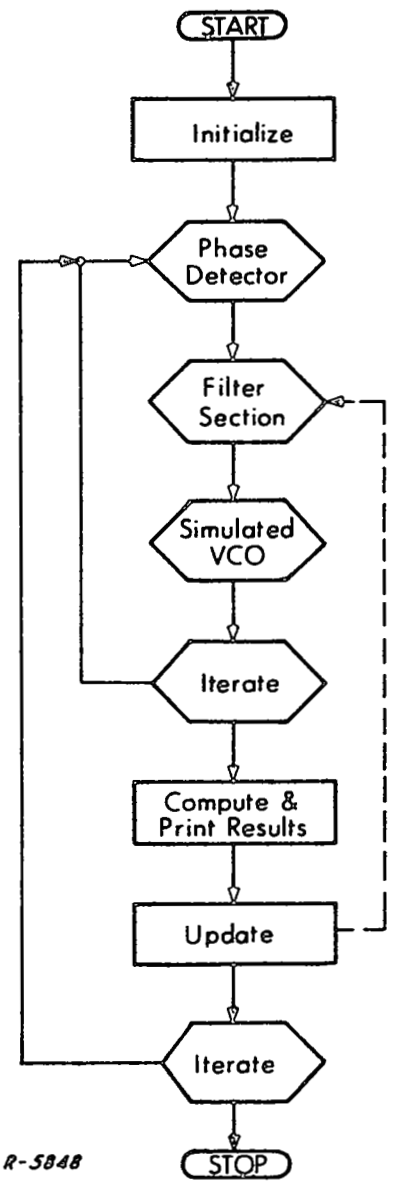

Fig. 14 "Photon" Program

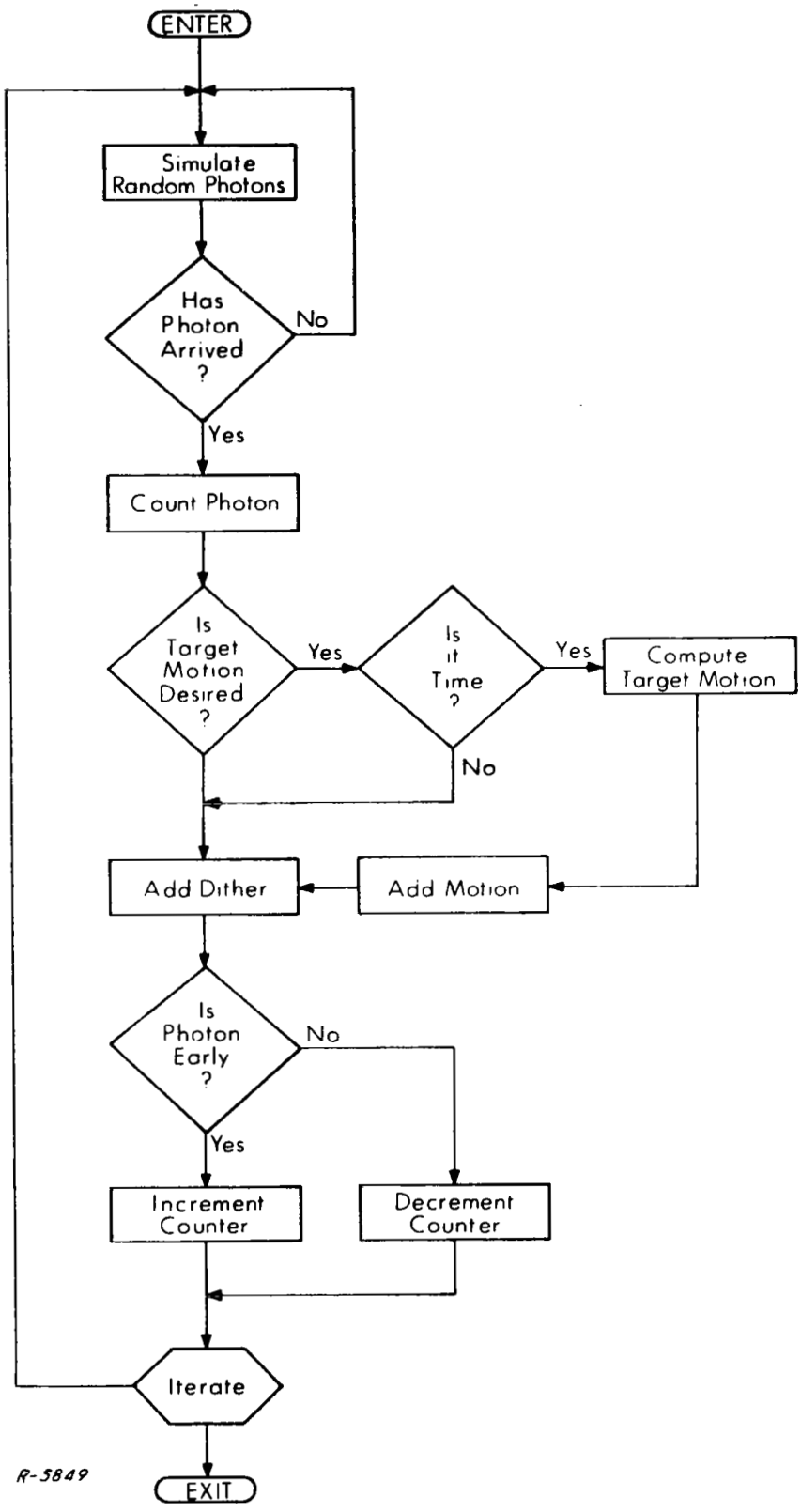

Fig. 15 Phase Detector Simulaton

If the target motion switch has been enabled (ISW = 1) and the transition point has been reached (IP = current iteration), then the equation of motion (a quadratic) is evaluated and summed with the initial input signal (OFFSET) to obtain the input phase signal (PSI).

Then the error signal (ERR) is computed and summed with a randomized loop dither (EPS). Counter K is incremented or decremented depending on whether the resultant error is positive or negative. Counter K remains unchanged until a photon arrives (i.e., counter J is incremented) or until the end of an iteration of the main loop. The value of K is then normalized by dividing by J, the result becomes the update (COUNT) for the next iteration, and both counters are re-initialized to zero.

Every 250 iterations, the phase detector routine hands off to the phase-locked loop routine for the filter and VCO computations.

Phase-Locked Loop

The Phase-Locked Loop section is shown in Fig. 16. When the program is initiated the phase-locked loop has a second order filter configuration (ACC2, SUM2). If the program has progressed to the desired point (LP) the filter constant (TAU) is changed, and an additional filter section is switched in (ACC1, SUM1, GAIN2P). In either event the update (COUNT) obtained from the previous iteration of the main program loop is accepted and operated upon. Operations on the update by each section of the filter consist of accumulation, multiplication, and summation as shown in Fig. 16.

The output of the filter is fed to the VCO accumulator (ACC3) whose output (modulo 2π) is the local oscillator phase signal (PHI). Every 20 iterations, the phase-locked loop hands off to the main loop for computing the update and for printing time (M), photon count (J, K), error and running mean errors (AMU, RMS).

Using the Program

Tables 1 and 2 summarize the input parameters required by the program and the results which are printed out at one second intervals.

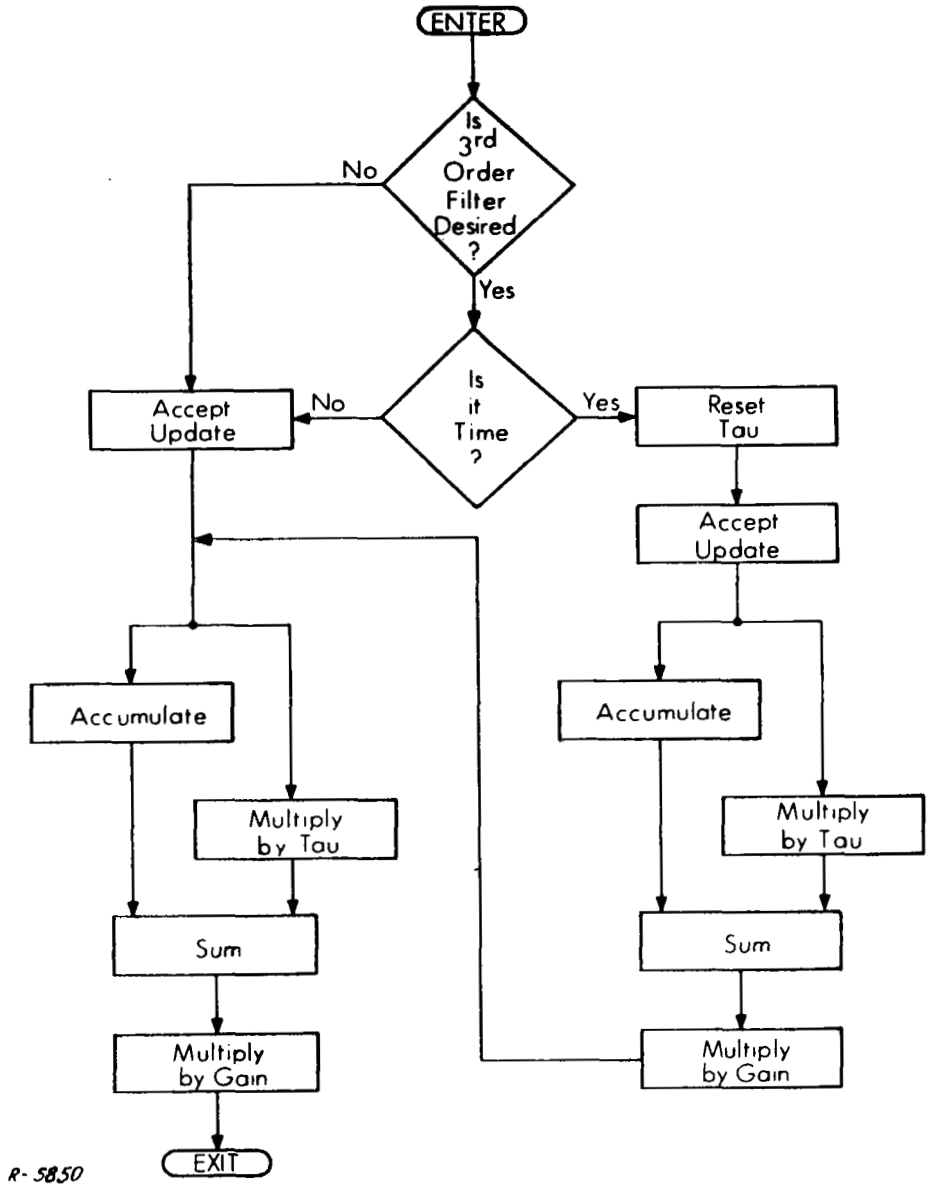

Fig. 16 Loop Filter Simulation

Table 1

NAME	DESCRIPTION
ITER	Number of main loop iterations. One iteration is equivalent to one real time second.
IX, IY	Random integers required to initialize subroutine RANDU. The magnitude of both integers must be non-zero and less than $2^{15}-1$.
MPHI	Mean photon arrival rate (per second).
ISW	Switch to enable (=1, disable ≠2) introduction of target motion.
LSW	Switch to enable (= 1, disable =2) change to third order filter.
JSW	Switch to enable (= 1, disable =2) acquisition sweep.
MPIP	Iteration or time (in seconds) if and when target motion is to be introduced.
MPLP	Iteration or time (in seconds) if and when third order loop is to be introduced.
EPSJ	Magnitude of the instrument induced jitter at the receiver gate (in feet).
T2ND	Filter factor for the second order loop configuration.
T3RD	Filter factor for the third order loop configuration.
G2ND	Gain factor for the second order loop configuration.
G3RD	Gain factor for the third order loop configuration.
ACCEL	Two-way* target acceleration coefficient (in feet/sec^2).
VEL	Two-way target velocity coefficient (in feet/sec).
RANG	Two-way target range coefficient (in feet).
STEP	Initial offset in two-way target range (in feet).

* The "two-way" range, velocity or acceleration of a vehicle is the range velocity or acceleration seen by the tracking receiver, e.g., a vehicle with absolute velocity V produces a doppler given by $2Vf_o/c$ where 2V is the two-way velocity.

Table 2

NAME	DESCRIPTION
TIME SEC	Program run time in real time seconds equivalent to one iteration of the main program loop.
PHOTON SUM	Number of simulated photons arriving during the one second iteration.
PHOTON DIFF	The difference between those photons arriving early and those arriving late relative to the local oscillator phase signal.
PHOTON RATIO	Photon difference divided by photon sum.
ERROR IN FEET	Two-way range error in feet, i.e., absolute range error = "error in ft/2."
RUNNING MEANER	Running mean of the two-way range error (in feet).
RUNNING RMS ER	Running RMS two-way range error (in feet).

Results

A typical computer printout obtained with the PHOTON program run on a SEL 810B computer is included in Appendix A. The system is simulated to have second and third order B_n = 0.1 Hz, a mean input signal photoelectron rate of 3 per second and the target is simulated to have a two-way acceleration of 1.4×10^{-2} ft/s. The resulting two-way rms range error is around 1.5 ft. (0.75 ft, one-way). A bias error of 0.5 ft. was observed for the entire 180 second run. In theory, there should be no bias error under the simulated conditions. It is expected that had the run been continued for several more minutes, the running mean error would, in fact, have reduced to zero.

SECTION 6
TRACKING GATE DESIGN

This section is devoted to the design and implementation of split-gates and leading-edge gates. First, the design of split-gates with gate widths on the order of 1 - 20 nsec is discussed. Then the design and implementation of extremely narrow gates (< 1 μsec) are discussed. A laboratory effort is described in which several of the gate implementation concepts were tested. The section concludes with a discussion of special considerations relevant to the design of leading-edge trackers.

Split-Gate Design

Both the MSL altimeter and the lunar ranging device considered in this report employ the split-gate tracking technique. The role of the split gate in such tracking systems is described in Sec. 2. The photo-multiplier which drives the loop is described as follows:

1) Output impedance is 50 Ω

2) Output pulse for single photon event has constant energy

3) Desired P. M. output for single photon event is Gaussian in shape with amplitude ≥ 300 mv (preamplification may be employed).

Narrow (1-20 ns) Split-Gate Design

The detection circuit for moderate width split gates may take two equivalent forms, typically the system shown in Fig. 17 is used. Due to

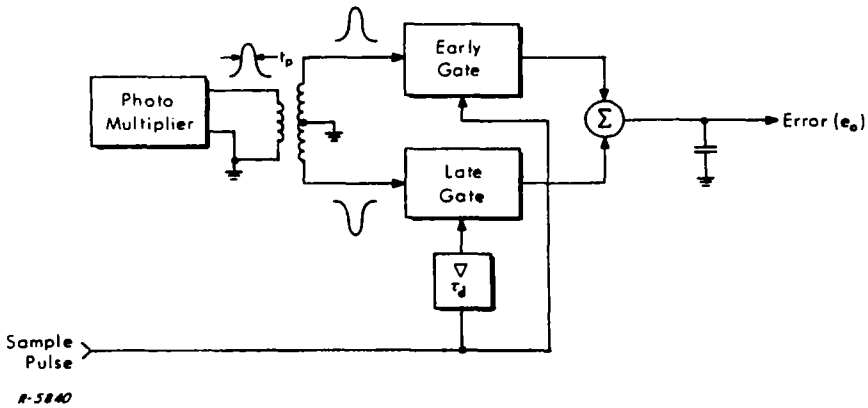

Fig. 17 Split-Gate Detector

the uncertainty of MSL caused by swells, the decision gate must observe a greater time interval than the expected pulse width. The error signal will be linear over a small time interval, corresponding to the received pulse width. Throughout the remaining window, the error signal will be ±1, as shown idealized below.

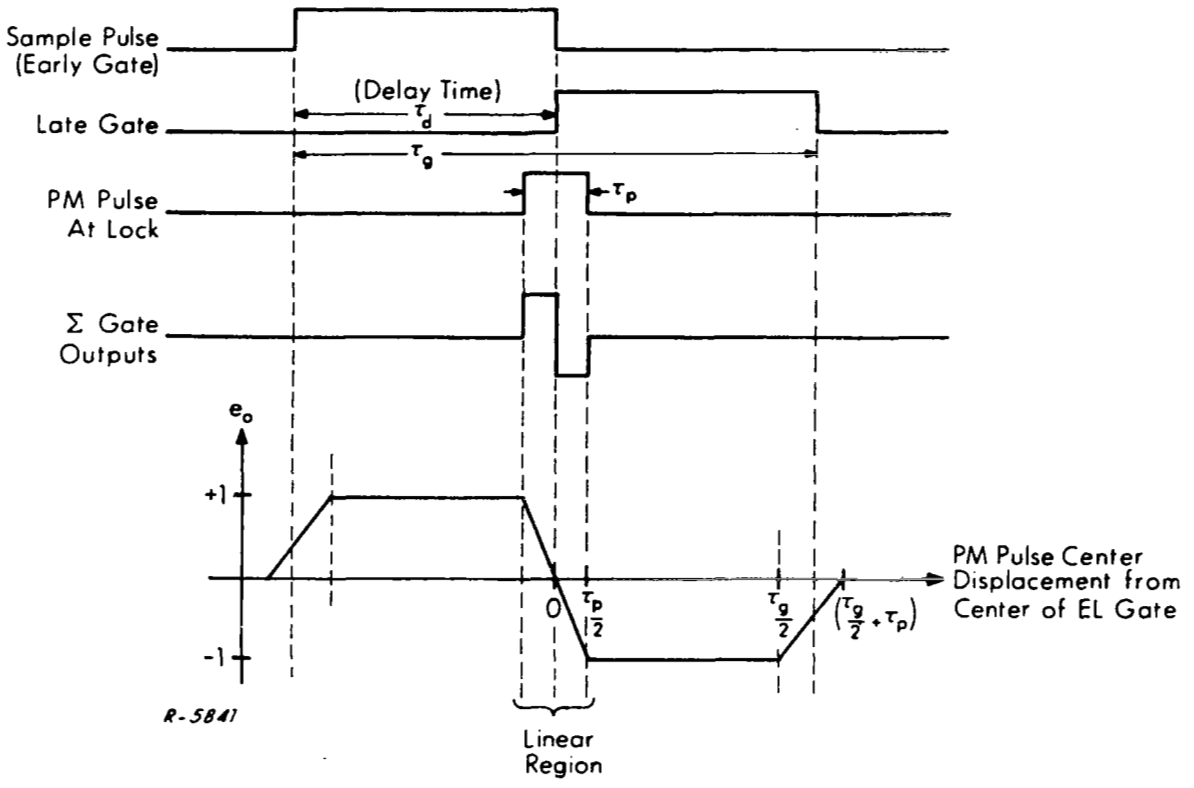

An equivalent detector can be built using a single gate element. In this case, the inverted P. M. pulse is first summed with a delayed positive version of the P. M. pulse. The delay required is $\tau_g/2$. An idealized block diagram and timing illustration is given in Fig. 18.

The latter circuit is simpler and more economical to implement. A single gate eliminates the need for critical matching necessary in the two-gate system. Analog delay at very high bandwidths is possible using precision coaxial cables. The inversion of a P. M. pulse can be easily

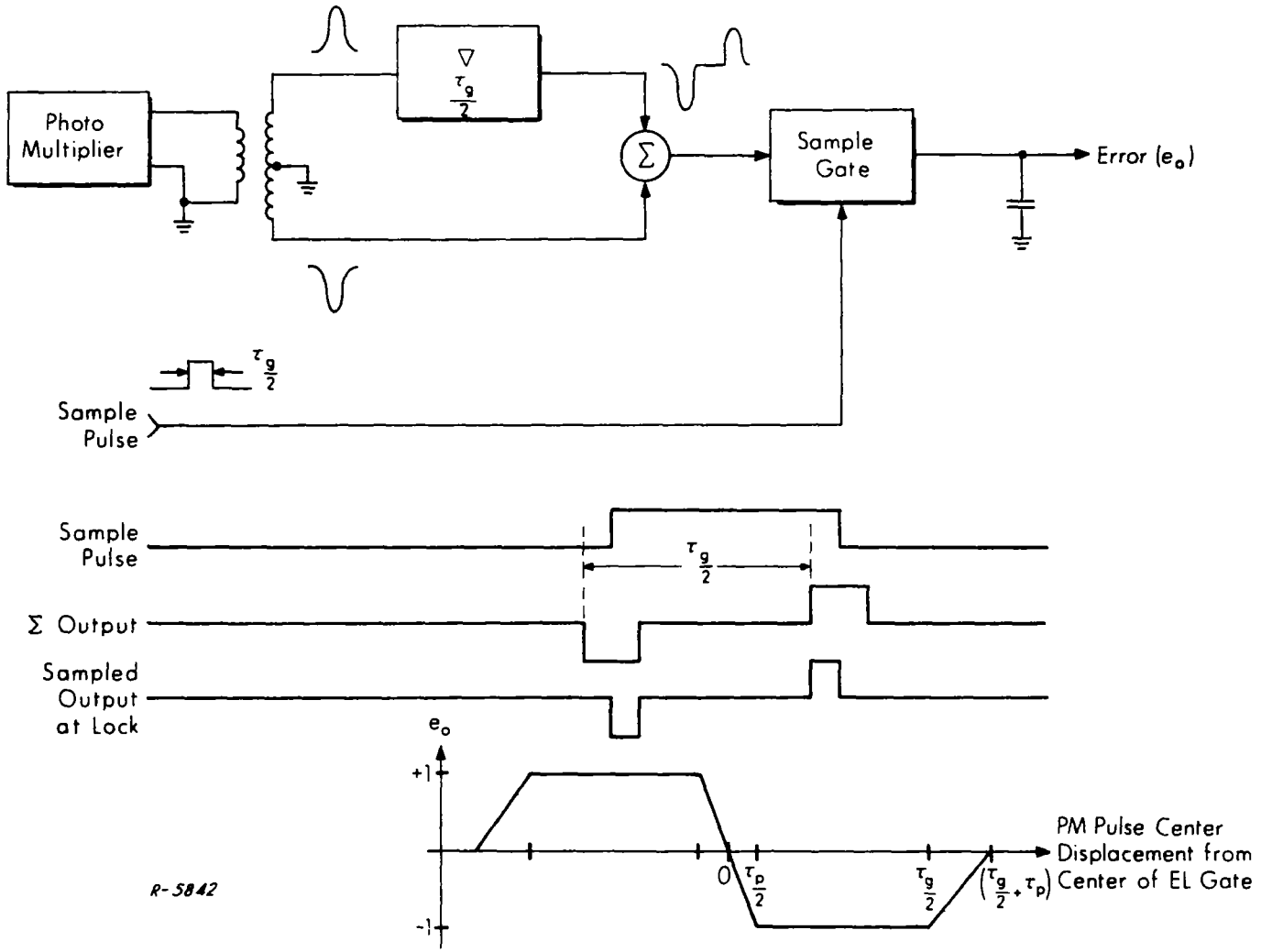

Fig. 18. Alternate Split-Gate Circuit

accomplished using commercial 180° hybrid junctions such as the ANZAC H-8, having BW from 1 MHz to 2 GHz, with < 1.0 dB insertion loss over the band. The video summing is performed with a UHF broadband power divider or a second hybrid junction operated as a summer.

The sampling gate is the remaining concern. Hewlett-Packard (and others) makes a broadband double balanced mixer which can be used as a pulse modulator or sampling gate to 500 MHz. Rise and fall times of the gate are 1 ns. Sampling rates are DC to 500 MHz (from specification sheet for H. P. #10514A Mixer).

Laboratory Experiments

A laboratory breadboard effort was conducted to determine the limitations of standard printed circuit techniques and commercial components in building a video gate. Of primary concern were sample gate width and maximum repetition rate. The circuit given in Fig. 19 was used in the tests. The diodes, Solitron MS7330, are metal-silicon junction diodes with reverse recovery times $\approx$ 0.5 ns. Other gate diodes with faster switching times are available, including H. P.'s hot carrier diode line with minority carrier lifetime as low as 100 picoseconds. The H. P. diodes will provide shorter turn-off times. Motorola emitter coupled logic (MECL III) is used to improve trigger transition times.

The video gate is triggered by a negative transition. Shaping is performed in the two gates which improve the risetime to 1 ns. Prior to the negative transition, diode D1 is conducting. As the anode of D1 goes negative, a current spike is coupled to T1 turning on the bridge circuit. On completion of the negative transition, the field in T1 collapses, back biasing D1 and creating the turn-off transition for the bridge. The characteristics of T1 (and its loading) define the turn-off transition and gate width. As indicated in the drawing, three different transformers were tested at T1, providing three different gate widths. Figure 20 shows the gate waveform characteristics. Since gate turn-off is related to pulse width, the narrower gates performed best. When the gate width is 3.8 nanoseconds, rise and fall times are 0.5 and 2 nanoseconds, respectively. At 12 nanoseconds τ_g, tr = 1 ns, t_f = 3 ns, and at 20 nanoseconds τ_g, tr = 3 ns, $t_f \approx 6$ ns. It is noted that this circuit is limited as to maximum gate width due to the turn-off mechanism. In the region between 3.8 and 12 ns, the circuit is satisfactory as a sample gate. Maximum rate of operation is a function of the transformer-load time constant. Gate width is independent of sampling frequency for sample rates less than 8.5 MHz in the 12 ns gate.

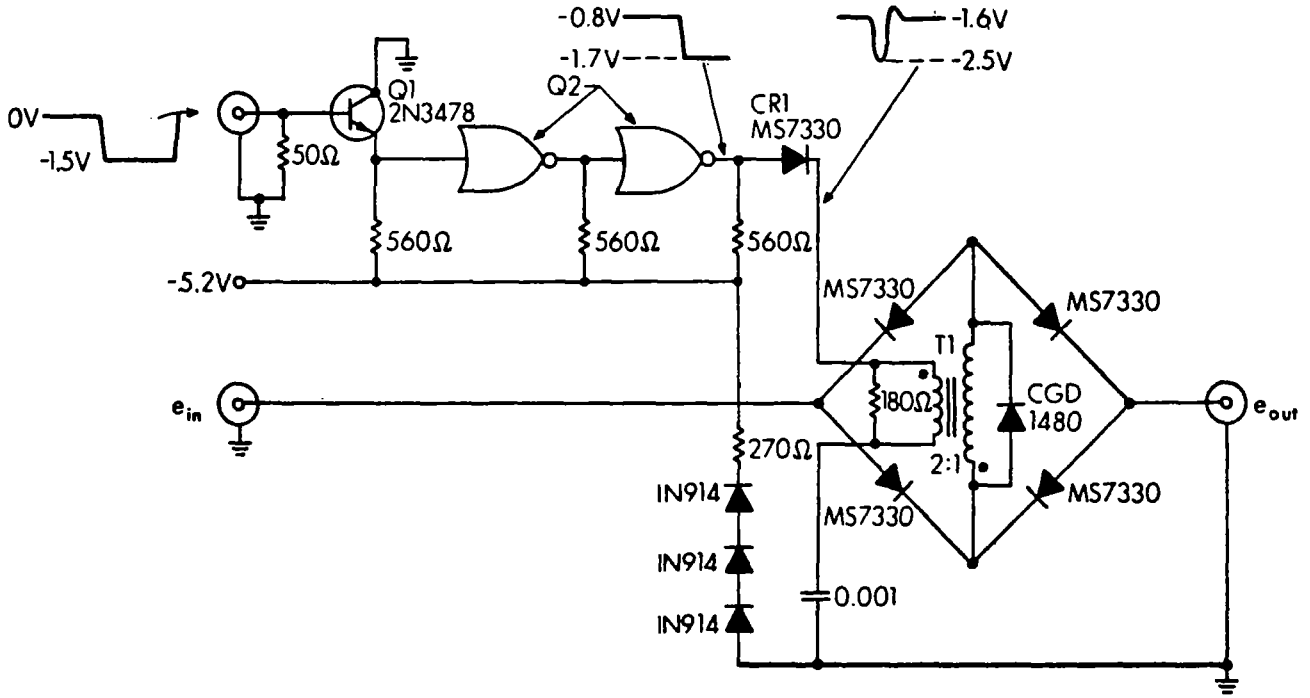

T1: Core Material-Ferroxcube K5-050-40/1Z2		
Gate Width	Winding Data	L_p
3.8ns	Pri: 3T #30 Sec: 6T #30	0.25μH
12ns	Pri: 5T #30 Sec: 10T #30	0.55μH
20ns	Pri: 8T #34 Sec: 16T #34	1.6μH

R-5843

Q2 - Motorola

Fig. 19 Video Gate

Fig. 20 Gate Waveform

If the sample pulse is made a very narrow negative pulse (less than the natural gate width of the T1 transformer), T1 will act as a wide-band pulse transformer, and the gate width will then be equal to the input pulse width. Using this mode of operation, the gate operated easily at 50 MHz, with a τ_g = 5 nanoseconds.

Considering the transmitted signal, stray capacities associated with the gate structure must be charged in addition to the output capacity of the gate. As the gate width is decreased, the fraction of analog signal actually measurable at the gate output becomes smaller due to the finite time constants involved. If the gate width is maintained constant, the output of the gate (charge or voltage) is linearly related to the signal input. The ratio of a change of output voltage to the responsible change of input voltage is the efficiency of the gate, for a given gate width. Observed efficiences were approximately 4% at 3.8 ns, and 20% at 12 ns gate width.

Leading-Edge Tracker

The leading-edge tracker is desirable when return pulse jitter is less than photo-multiplier risetime. This would occur with lunar ranging or atmospheric probes. In the case of MSL determination, the range uncertainty associated with waves would render a leading-edge tracker useless, and a split-gate system should be used.

A model of the video processing necessary for leading-edge tracking is shown in Fig. 21, with the resulting idealized waveforms. Realization of the circuit is straightforward. The transformer and summer utilize 180° breadboard hybrid juctions, such as Anzac #H-8. Precision delay cables, and precision attenuators to provide proper amplitudes complete the setup. Bandwidths can be maintained to 2 GHz with existing state-of-the-art components. The necessary sampling gate must operate with the period 2 Δt defining its linear region. It is anticipated that this period will be $\leq$ 1.0 ns as detected by the P.M. tube. The gate must be narrow compared to $2\Delta t$, thus restricting the technique to

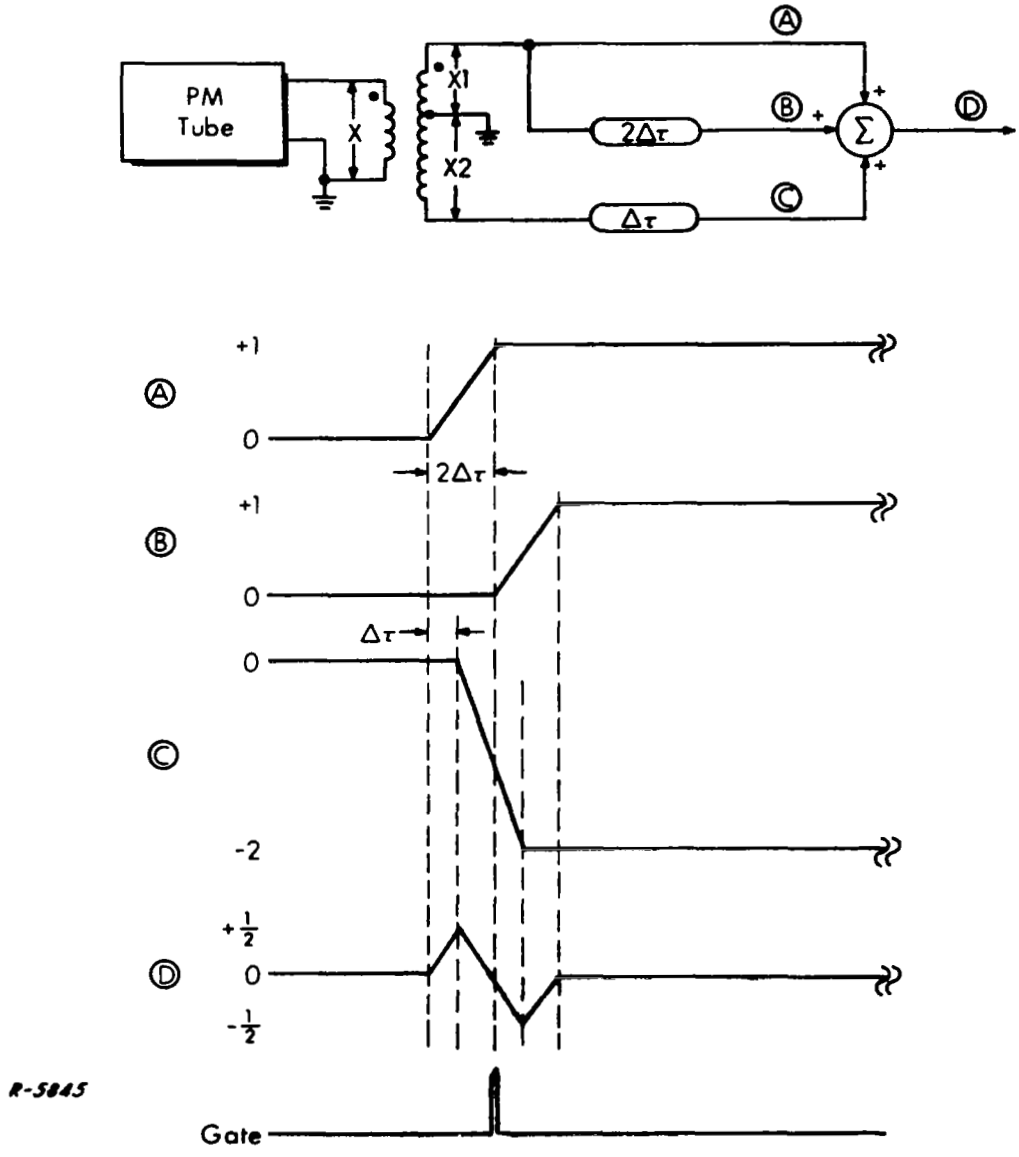

Fig. 21 Leading-Edge Tracker
(Video Processor)

that of the sampling oscilloscope. With the most recent advances in sampling oscillography employing monolithic gate structures, it is possible to obtain gate widths as low as 25 picoseconds. Other "standard" sampling windows are 50 ps, 90 ps, and 350 ps.

At these narrow sampler windows, the efficiency of such a gate (monolithic) is limited to about 0.2 to 0.5 percent due to stray capacities in the gate structure. To offset these losses, an error-sampled feedback technique is used. With this technique, the gate output is sensed by an AC memory circuit. Between samples the memory circuit, whose gain is determined by the sample gate efficiency, amplifies the error signal to affect unity gain through the gate. Memory output is fed back to the gate output so that the gate will indicate error only for a change in input signal. Utilization of this technique suffers from the limitation on sampling rate, which occurs due to the slow rate of the memory circuit. Typical maximum sampling rates are 100 kHz.

Investigation reveals that it is not necessary to purchase an entire sampling oscilloscope to obtain the necessary circuitry of the sampler. Tektronix sells two sampling plug-ins, 1S1 and 1S2 with 350 ps and 90 ps windows, respectively, which contain all the circuitry necessary to provide the triggered gate function. A plug-in unit power supply, #132 supplies the necessary power to these units. A small modification must be made to the unit to allow real time sampling with an external pulse command. Maximum sampling rate for all sampling units is 100 kHz. The output obtained from this type of gate is similar to that of a sample and hold circuit, maintaining the dc level of the previous sample until the next sample is taken. Since additional circuitry within the preamp is used to boost the sampler output to establish unity gain through the gate, the rise time of the output signal is not that of the gate, but of the servo amplifier following the gate. Typically, this (observed) rise time is 2 - 3 μsec. It is this amplifier which limits the sampling rate of the gate. In addition, the servo amplifier, with input bandwidth of 1 - 14 GHz, has output BW of 150 kHz while preserving amplitude information. In this form, the samples are ready for analog to digital conversion without further processing.

Should a narrower window be required, or the capability of several different windows with the same plug-in unit, the Tektronix 3S2 sampling unit, which accepts several plug-in sampling heads, can be used. The 3S2 unit requires more extensive modification for use as a leading-edge tracker gate. An external power supply must be obtained, and external sampler drive must be provided. The advantage of this unit is interchangeability of the sampling gates. Available are the following gates: S-1 at 350 ps., S-2 at 50 ps., and S-4 at 25 ps. All necessary strobe pulse-generating and shaping circuitry exists only once; only the physical gate structure and preamp are replaced with the individual heads.

A trade-off to be encountered is gate width vs. gate noise. As shown below, the wider gates have less inherent noise.

TYPE	RISETIME	NOISE
S-1	350 ps	2 mv
S-3	50 ps	6 mv
S-4	10 ps	10 mv

Output levels available from the plug-in units have source impedance of 10 kΩ, gain controlled by front panel attenuator control and output limit of ± 4 volts. Transient response varies from ± 10% for the S-4 to ± 0.5% for the S-1 gate.

SECTION 7

CONCLUSIONS

The results of the study effort indicate the feasibility of an optical MSL Altimeter employing a mode-locked laser transmitter and a phase-locked loop receiver tracking system. Noise and dynamic error characteristics were determined and tradeoffs performed. It was found that the required dynamic performance of the receiver system could be obtained while operating with narrow tracking bandwidths commensurate with input photoelectron rates approaching one per second and signal-to-noise ratios approaching unity. This performance was verified by a computer program which very accurately simulated the proposed tracking receiver design. A laboratory effort was conducted to verify that receiver input gating structure appropriate to the tracking receiver design could be realized given state-of-the-art, commercially available components.